NASA CR- 66297

ACTIVE OPTICAL SYSTEM

FOR

SPACEBORNE TELESCOPES

FINAL REPORT

N67 18968

PERKIN-ELMER

ELECTRO-OPTICAL GROUP   NORWALK, CONNECTICUT

ENGINEERING REPORT NO. __8525__

ACTIVE OPTICAL SYSTEM FOR SPACEBORNE TELESCOPES
FINAL REPORT

DATE: __OCTOBER 14, 1966__

PREPARED FOR: NATIONAL AERONAUTICS AND SPACE ADMINISTRATION

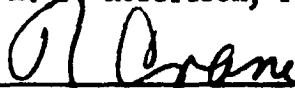LANGLEY RESEARCH CENTER

LANGLEY STATION

HAMPTON, VIRGINIA   23365

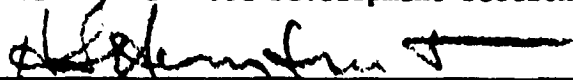CONTRACT NUMBER: NAS1-5198   PROJECT NUMBER: SPO 26940

H. J. Robertson, Project Manager

R. Crane, Advanced Development Section Manager

H. S. Hemstreet, Space Optics Department Manager

Contributors:
R.A. Arnold   R.C. Liu
R. Crane   D.L. Pillsbury
R.J. Fowski   H.J. Robertson
E.C. Gaal   R.A. Sprague
           D.T. Thompson

TABLE OF CONTENTS

LIST OF ILLUSTRATIONS

LIST OF ILLUSTRATIONS (Continued)

LIST OF ILLUSTRATIONS (Continued)

LIST OF TABLES

ACTIVE OPTICS DIFFRACTION IMAGES

Double exposure of pinhole images produced by the active
optics mirror assembly showing three images from three
segments prior to alignment; a single diffraction image
in the center from the composite mirror after automatic
alignment, and with control servos on.

1. SUMMARY AND CONCLUSIONS

It is becoming increasingly apparent that in the near future the large booster capability developed by the National Aeronautics and Space Administration (NASA) will make it possible to place in orbit a large telescope suitable for astronomical and other purposes. It is expected that the launching stresses, the thermal environment, and the change from gravity to gravity-free existence will make it very difficult to build a telescope using conventional techniques which can take full advantage of its size after reaching orbit. The purpose of the Active Optics Project is to derive optical techniques which will make it possible to perform corrections upon an optical system after it has reached its orbit so that diffraction-limited performance can be obtained from a very large orbiting telescope. The laboratory experiment described in this report has shown that it _is_ feasible to automatically align and control the figure of a primary mirror for use in a large optical telescope.

The fundamental concept of Active Optics consists of measuring the surface shape, or figure, of a telescope primary mirror, computing the necessary electronics control signals, and physically aligning the mirror to its original design figure. This experiment consisted of measuring and correcting the alignment of the individual elements of a segmented primary mirror. If truly diffraction-limited performance is to be obtained, this alignment must be done to an accuracy of 1/50 of a wavelength of light to be received, or to better than 1/2 microinch rms over the entire aperture for a visual telescope.

The specific objective of this experiment was to automatically align and maintain closed loop control of a 20-inch diameter, three-segment mirror, to 1/20 wavelength rms of the design figure. Figure 1 shows the experiment block diagram. A spherical figure was selected for simplicity. Two sensors were used for figure measurement; a fine figure sensor consisting of a phase measuring interferometer excited by a low-power laser, and a white-light equal-path interferometer for resolving the ambiguities due to the coherence of the laser source in the fine sensor. The electronics consisted of an image scanning tube for detecting the interferometer fringe pattern, an alignment analyzer, a small amount of control logic, and servo amplifiers. The mirror segments were positioned by motor-driven differential-spring actuators, three per segment. A major portion of the optical path was maintained within a vacuum tank to avoid the effects of air turbulence.

The project was divided into two phases: Phase I, to investigate and fabricate the critical elements of the experiment; and Phase II, to combine these elements into a control system that would demonstrate the feasibility of the Active Optics concept. Engineering data concerning component selection, design detail, and the results of component testing were reported at the completion of Phase I in Perkin-Elmer Engineering Report No. 8255. This final
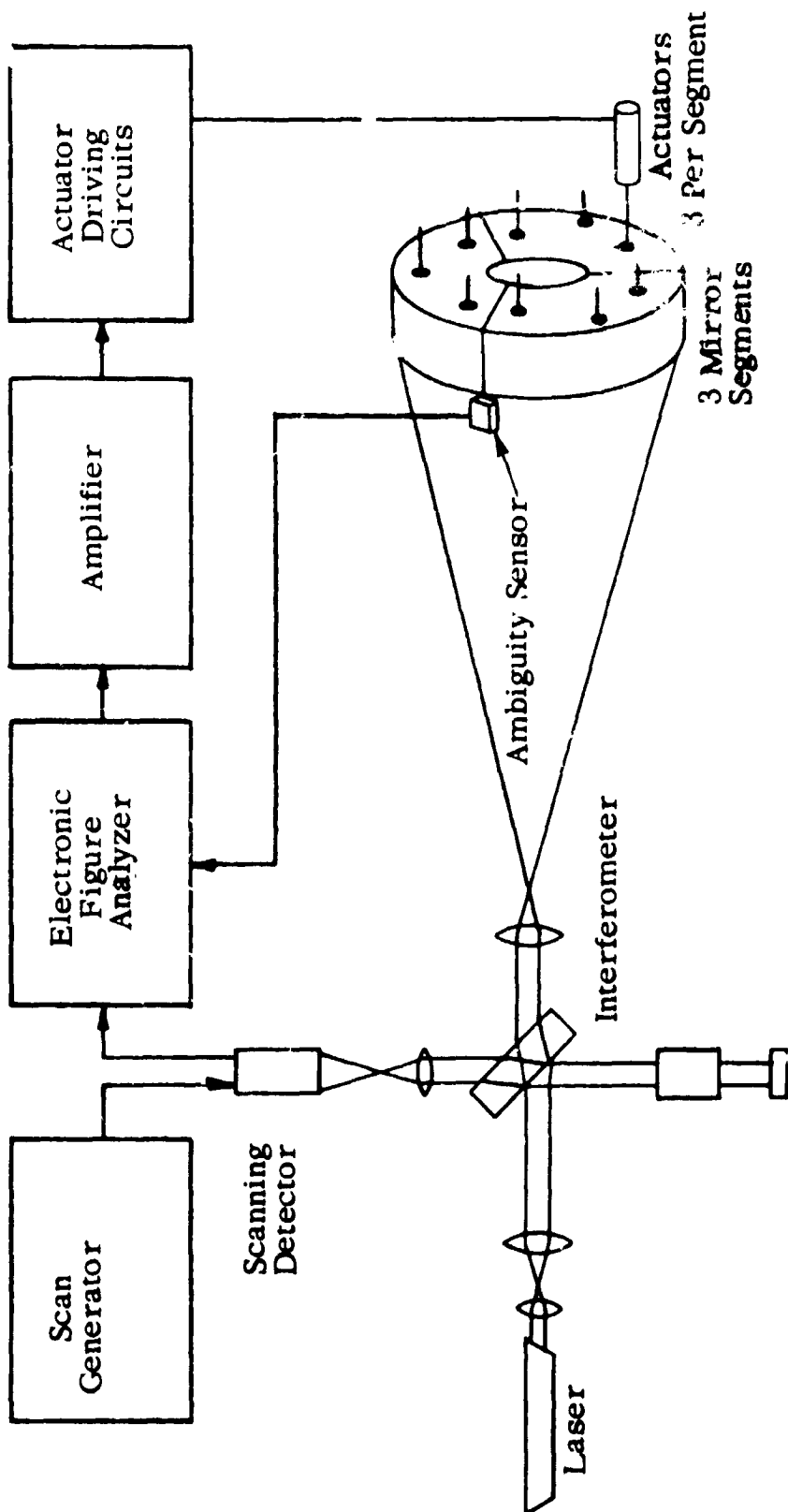
Figure 1.   Experimental Arrangement Used for "Active Optics" Evaluation

report presents a summary of the pasic objectives, descriptions of the components used in the laboratory experiment, descriptions of the closed loop operation, and examples of the data obtained in testing the overall assembly.

The results of this work have been most encouraging. The mirror figure before being segmented was 1/35 wavelength rms. The composite figure of the segmented mirror assembly after automatic alignment, and measured while closed-loop control was in operation was better than 1/30 wavelength rms of the design figure. Dynamic response was approximately 3/4 cycle per second with dynamic stability better than 1/100 wavelength rms. Numerical estimates of alignment accuracy and limiting factors for segment tilt and axial positioning are given in Table IV, on page 66 of this report. Examples of figure error profiles, knife-edge test data, and interferometer fringe patterns before and after alignment, are given in Section IV of this report. The frontispiece contains a typical set of pinhole image photographs showing three images produced by the three segments prior to alignment and a single image produced by the composite mirror after automatic alignment. These pictures were taken with the control system in operation. The same exposure and magnification were used for all images in this picture to demonstrate the decrease in size of the diffraction image produced by the larger diameter mirror which resulted from aligning the three segments to a common spherical surface; thus proving that diffraction-limited performance can be obtained by automatic alignment of a segmented mirror.

2. OBJECTIVES

The steadily increasing interest in astronomical observatories out-
side the earth's atmosphere and the future needs of deep-space optical communica-
tion systems make it apparent that there will soon be a need for very large
diffraction-limited telescopes suitable for operation in a satellite. Recently,
this need was identified by members of the Space Science Board of the National
Academy of Science and NASA who met at Woods Hole in the summer of 1965. Among
the recommendations of this study group were

"Recommendation 8

We conclude that a space telescope of very large diameter, with a
resolution corresponding to an aperture of at least 120 inches,
detecting radiation between 800Å and 1 mm, and requiring the capa-
bility of man in space, is becoming technically feasible and will
be uniquely important to the solution of the central astronomical
problems of our era. We recommend that the Space Science Board of
the National Academy of Sciences appoint an ad hoc panel to work
toward this Large Orbital Telescope and to encourage studies of
those critical areas where particular research and development is
required in the near future to further this program . . . . . ."

"Recommendation 6

We recommend that NASA be urged to support basic research and
development leading to the optimum design and construction of
space telescope optics. The vital areas are:

    (iii)   Methods for rapidly evaluating mirror figure and
            alignment under normal and zero gravity.

    (iv)   Methods for generating and maintaining diffraction-
            limited mirror quality in space, by passive or active
            means . . . . . "

The nature of the problem can be better understood by establishing
quantitative definitions for the term "diffraction limit" and by postulating
the major sources of primary mirror distortion. This was done in the Phase I
report where it was shown that for a small-scale and random figure error of
1/20 wavelength rms, the image from a star will have an intensity of 60% at its
maximum relative to that which would be produced by a perfect telescope of the
same size. Thus, a truly precise telescope should have a figure even better
than 1/20 wavelength rms. Dynamic rate and transient response are equally
important. For example, a differential thermal change in the telescope support

structure of less than 1°C per hour between two sides of a telescope can conceivably produce relative displacements between portions of a large optical system on the order of 1 microinch per second.

The concept of active manipulation of an aperture used for collection of electromagnetic energy is not new. Radio astronomers have been using the technique for some time; however, this is one of the first times the concept of automatic control has been applied to a large optical system. Figure 2 shows the basic approach applied to a segmented primary mirror. The necessary components consist of a mirror figure sensor, electronic error computer and control logic, and actuators for making necessary corrections to the optical element alignment. The corrections may be made by positioning individual segments of a primary mirror as shown in the Figure 2, or by mechanical deformation of a single, relatively thin mirror. For this project, the segmented approach was selected because it provided the possibility of demonstrating the feasibility of the basic concept with a minimum of subordinate problems.

The experimental arrangement for this project has been shown in Figure 2. Two sensors are used: a laser-illuminated Twyman-Green interferometer is used for detecting small tilt and focus alignment errors; a white light illuminated, equal-path interferometer is used for resolving integral wavelength ambiguities encountered in the fine sensor due to the coherent nature of the illumination. Coarse tilt alignment was done manually during the experiment. A possible scheme for automatic coarse alignment is described in this report (see Page 23), but was not tested in the laboratory; this was felt to be a less critical problem. The control electronics consists of an image scanning detector, scan generator, figure analyzer, and the necessary power amplifiers to drive the actuators. The image scanner samples the interferometer fringe patterns from all three segments. Logic circuitry then generates error signals for the control of the individual segment positioning actuators. Three actuators are used for each segment. These are located to permit orthogonal control of tilt. Axial adjustment is made by driving the three actuators in parallel.

It is believed that a peristaltic actuator is most appropriate for this application, especially where spaceborne operation is anticipated. However, for the laboratory experiment, a motor driven differential spring actuator was used in order to minimize special development.

The specific design objective of this project was to assemble the three segments and automatically adjust their alignment to within 1/20 of a wavelength rms of the design figure. A spherical surface was selected for economic reasons, although the technique is equally applicable to aspherical surfaces. Only individual alignment operations were to be automated; sequencing from one step to the next is manually controlled.
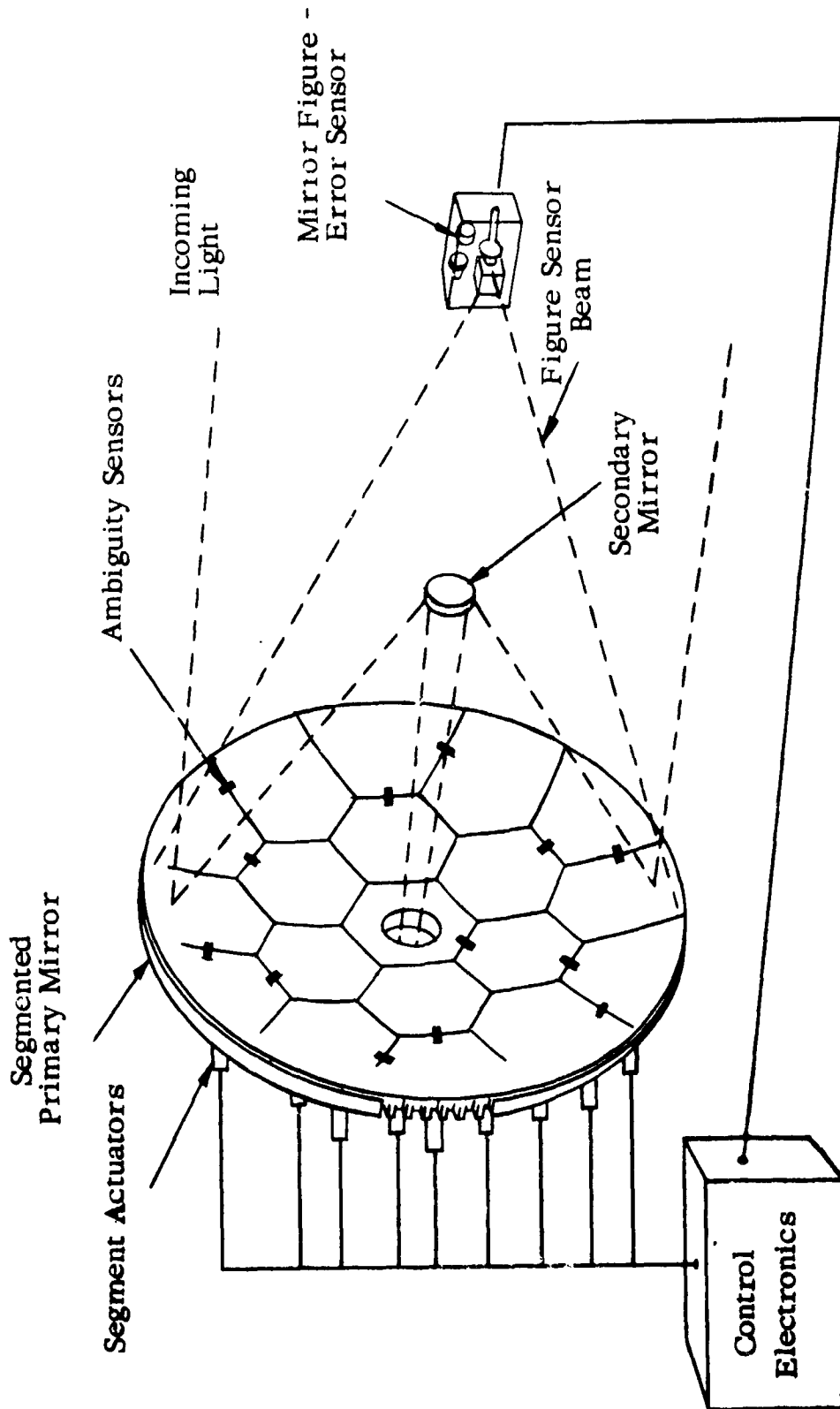
Figure 2. Active Optics Concept

Mirror Figure - Error Sensor

Incoming Light

Ambiguity Sensors

Figure Sensor Beam

Secondary Mirror

Segmented Primary Mirror

Segment Actuators

Control Electronics

6

The specific results required by the contract "Scope of Work" are described on the following pages:

3. COMPONENTS

3.1 MIRROR

To prove the feasibility of the concept of active control, mirror segments were required which would not seriously limit the performance of the closed loop system. A figure of 1/20 wavelength rms was considered sufficient for the purpose and it was not deemed necessary to invest the time and money required to figure a mirror to the λ/50 rms desirable for truly diffraction-limited performance. Therefore, less than λ/20 rms error was the design objective for the figure of the individual mirror segments.
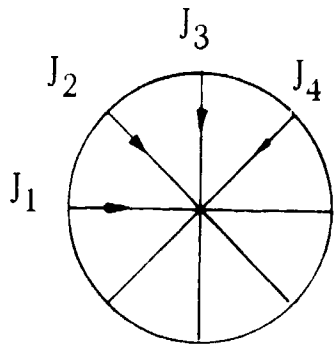
For the 20-inch diameter segmented mirror to be used in the feasibility demonstration, the simplest approach was to figure a 20-inch mirror and then cut it into segments. For a larger system the segments would not be cut from a larger piece but would be fabricated individually. Some of the problems involved in the fabrication of off-axis aspherical segments are discussed in Section 5 "Recommendations" on Page 67.

A 22-inch diameter fused silica blank was obtained with a minimum of internal stress, as indicated by less than 5 millimicrons birefringence, in order to reduce the possibility of warping when the mirror was cut.

The mirror was figured spherically with a 160-inch radius of curvature. Figure measurements were made before cutting to make sure that the error was less than the λ/20 rms objective and to make it possible to determine the effects of cutting. Profiles of the mirror before segmenting, obtained by computer reduction of data obtained from scatterplate interferograms, are shown in Figure 3. Peak figure errors here are on the order of λ/20 and the computer calculated rms figure error is λ/35.

The mirror was cut into three equal segments and measurements were made to determine the effects of cutting. These tests were made by an equal path interferometer and a scatterplate interferometer. Full circular fringes, as were used in the scatterplate tests before cutting, could not be easily reduced to profile information for the individual segments. The measurements were made instead from straight line fringes as shown in Figure 4. Fringe straightness and spacing give the information required to determine mirror figure error. The limit of accuracy of these tests was approximately λ/20. Although they indicated that the rms figure error of the segments was still less than the design objective of λ/20, quantitative information about the figure on a scale smaller than this was not consistent due to the effects of turbulence. A slight amount of warping was evident as can be seen in the composite knife-edge photograph in Figure 5, affecting primarily some of the segment corners and the cut edges. The magnitude of this warping was not sufficient to seriously degrade the rms figure.

The dimensional specifications for the mirror segments are shown in Figure 6. The amount of material removed between segments was partly dictated by the need for bracket space for the white light interferometer Koesters prism. The final width of the cut after dressing the edges was 3 mm, and this, together with a slight bevel at the edges added up to a 4 mm spacing between the mirror surfaces of the individual segments.
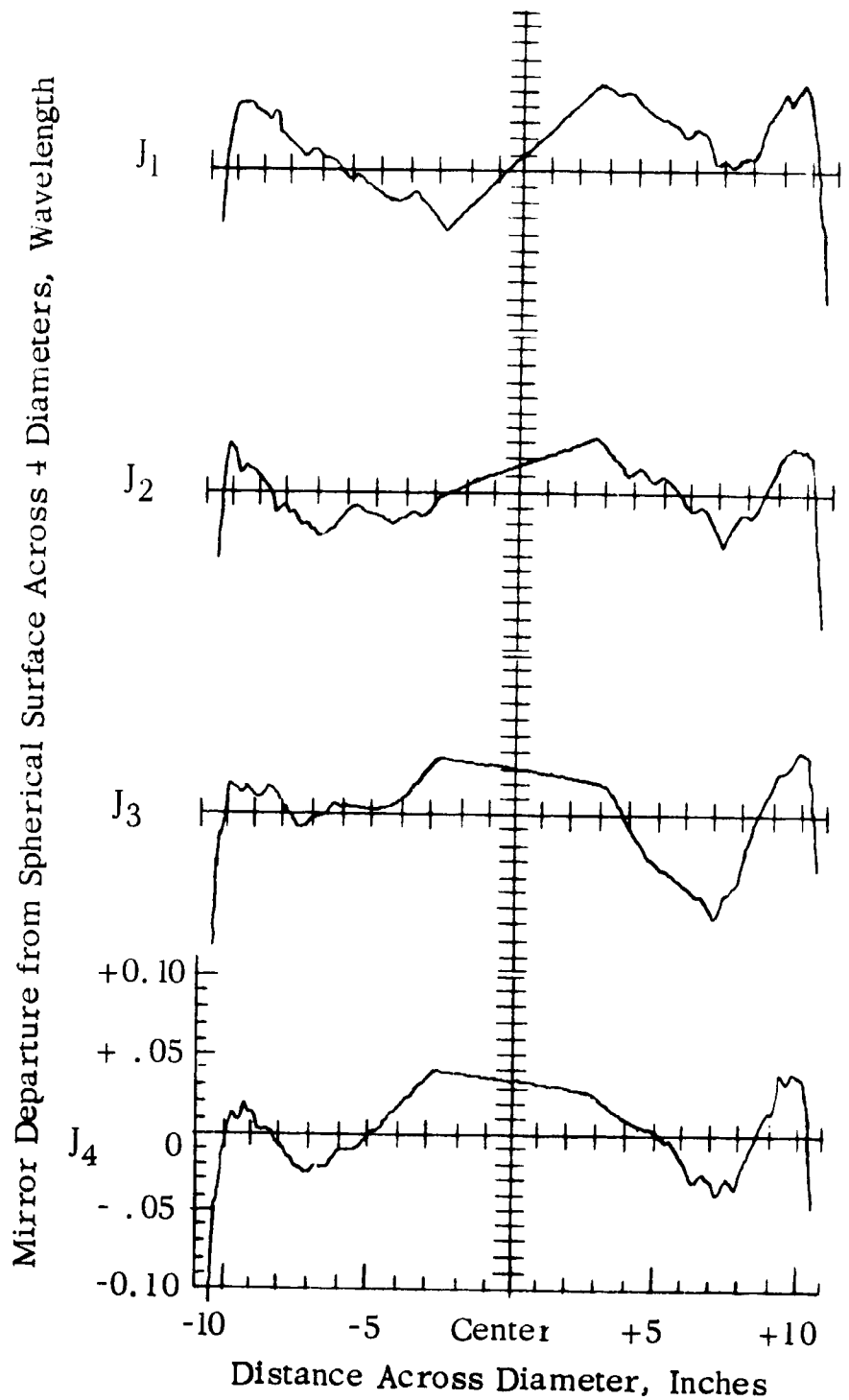
Figure 3. Figure Error Profiles Determined From Scatterplate Fringe Pattern at Mirror Before Segmenting. (rms Figure Error = $\lambda/35$)

Figure 4. Segmented Mirror Interferometer Data

Interferogram of mirror segment taken with scatterplate interferometer. Linearity and spacing of fringes are measured to determine quality of segment figure. Measurements show that the rms figure error is less than 1/20λ.
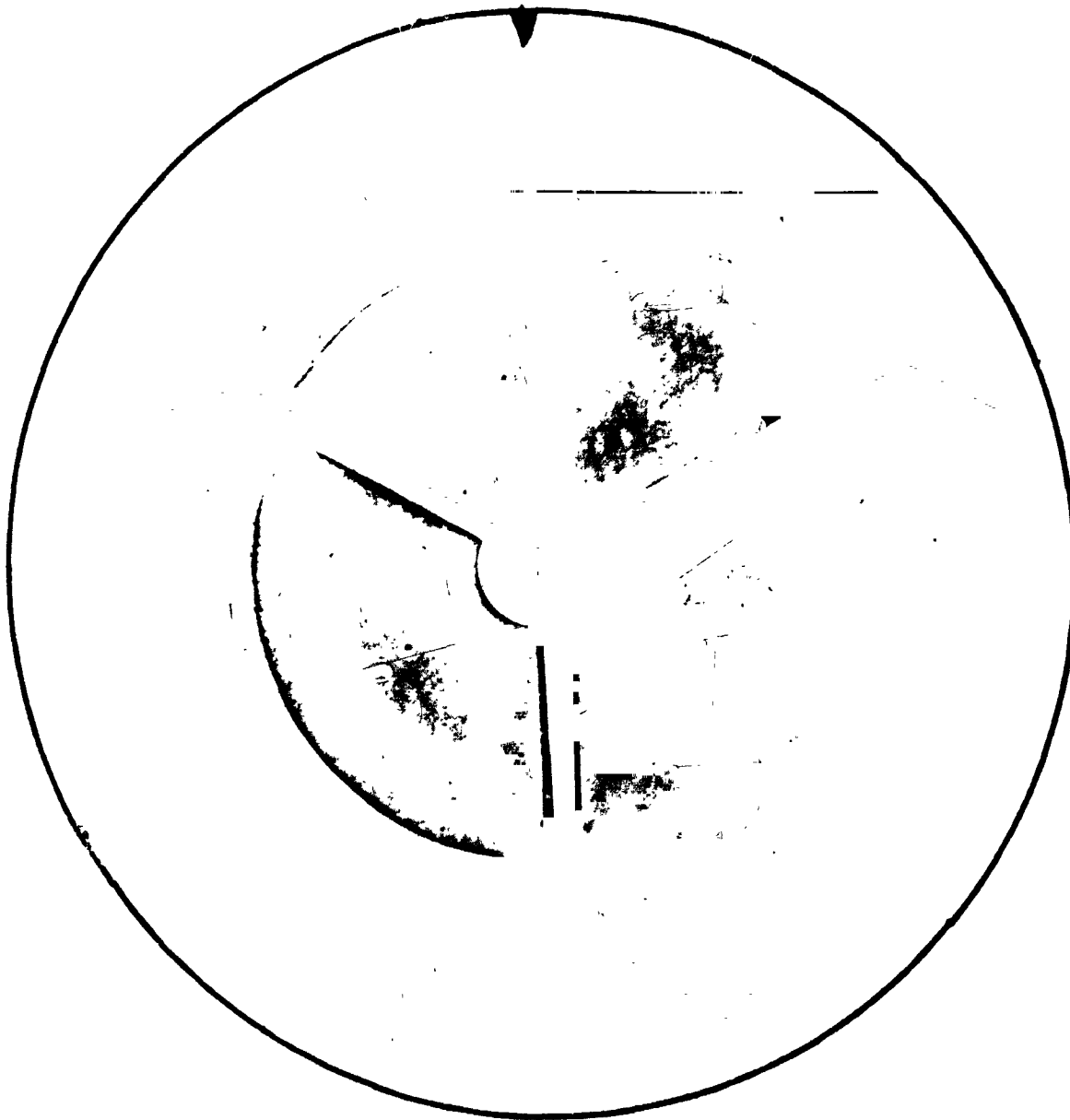
Taken individually and placed in proper position. Some warping
can be seen at segment corners but amplitude is small and overall
segment figure has not been seriously degraded by cutting operation.

Figure 5. Knife-Edge Photos of Segments

All Dimensions in Inches Unless Otherwise Specified

Radius of curvature 4065.0mm to $\frac{\lambda}{20}$ at 6328Å over 20" diameter
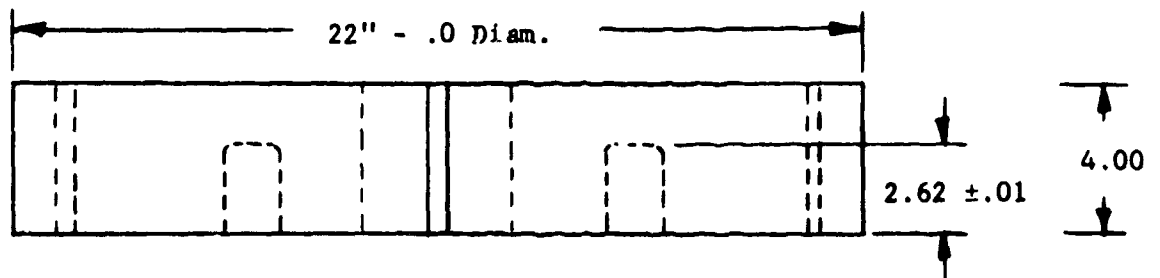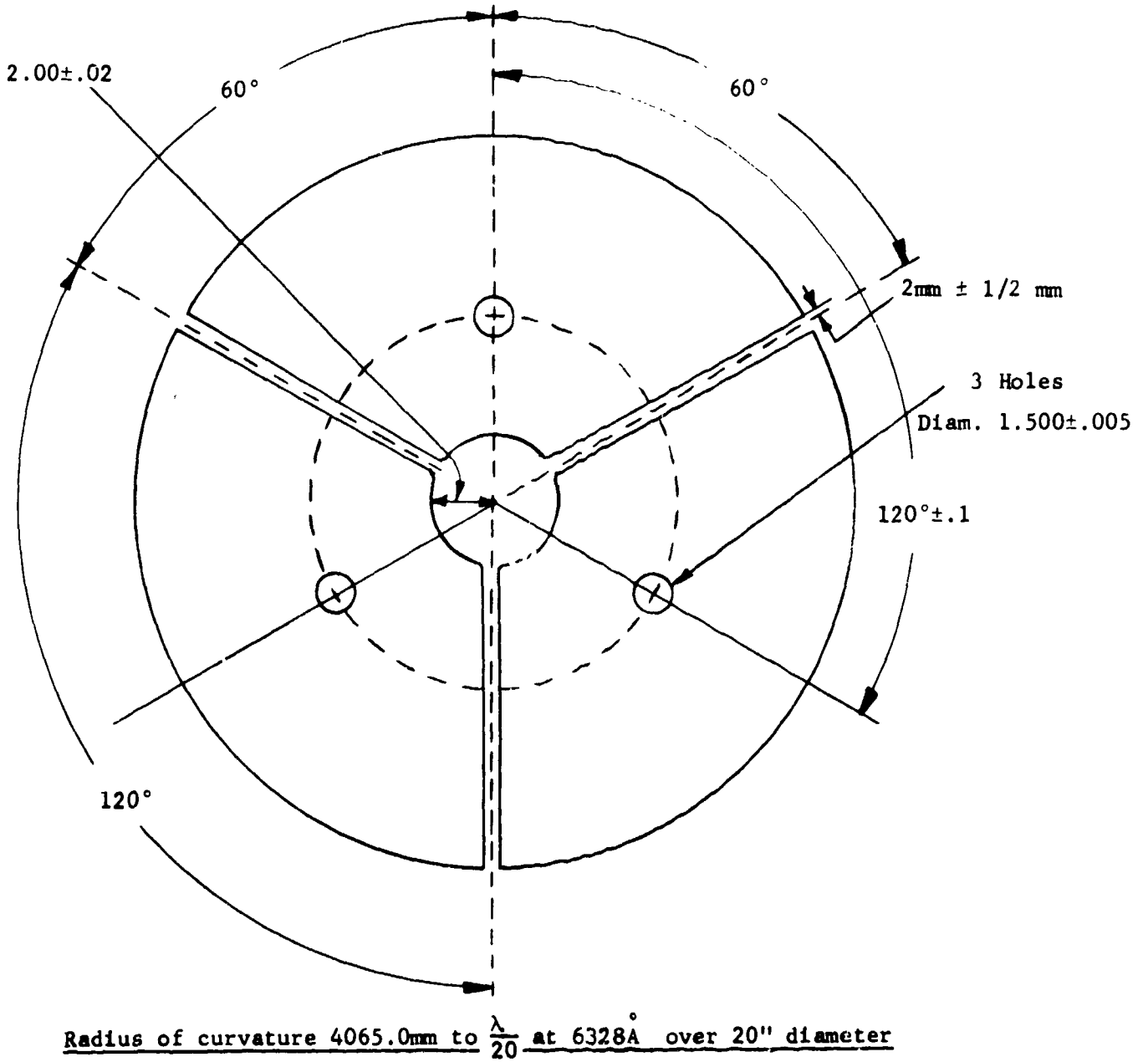
Figure 6 · Mirror Fabrication Specifications

3.2 SENSING DEVICES

3.2.1 Figure Sensor

A figure error sensor is required to examine each mirror segment surface and determine its relative position with respect to a section of a perfect spherical shell. The figure sensor should have a static accuracy and dynamic stability much better than 1/20 wavelength rms, and a dynamic range of at least 50 wavelengths. The response time should be compatible with a one cycle per second frequency response for closed loop alignment operation.

Optical interferometers are best suited for this type of measurement. Several varieties were compared in the Phase I study and a modified form of a Twyman-Green interferometer was selected. Figure 7 shows the arrangement used in the experiment. In this interferometer, two plane wavefront beams are formed from a common coherent source. One beam is reflected from a plane reference reflector; the second beam is converted from a plane wavefront to a converging, and then diverging spherical wavefront. This is done by lens-1 as illustrated in Figure 7. The diverging wavefront is directed at the mirror under test. If the mirror has a spherical surface and is aligned so that the center of curvature is located at the center of divergence of the wavefront (point "C" in Figure 7) the light will be reflected back exactly upon its incident path. It will then pass through lens-1 and again become a plane wavefront; thus, for a perfect spherical mirror, interference takes place at the beamsplitter between two co-planar wavefronts.

When there is surface irregularity in the mirror under test, the return wavefront will not be perfectly spherical and, hence, will not be co-planar at the point of interference. For tilt misalignment, the interference wavefronts will be plane but not parallel, producing a fringe pattern consisting of straight lines. For axial misalignment, interference will take place between a plane wavefront and a slightly spherical wavefront. This produces a circular fringe pattern. Thus, there are two unique, and readily recognizable signatures produced for the two types of misalignment anticipated. It is then the job of the scanning detector and electronics to recognize the presence of lines and/or circles in the fringe pattern and generate error signals from these signatures for the control of the segment actuators.

An additional element has been added to the interferometer to facilitate the electronic measurement of the fringe pattern. The accuracy needed for the figure sensor demands an ability to recognize not just lines but small fractions of a line in the fringe pattern. This is very difficult to do purely on the basis of intensity. Therefore, a phase shifter has been added to the reference arm. This device creates a continuously increasing phase shift between the two wavefronts at the point of interference. Therefore, the fringe pattern for perfect alignment cycles between uniform bright; that is, constructive interference between two plane wavefronts, and uniform dark, destructive interference. The photodetector therefore produces an electronic sine wave of identical frequency and phase for all points within the beam.
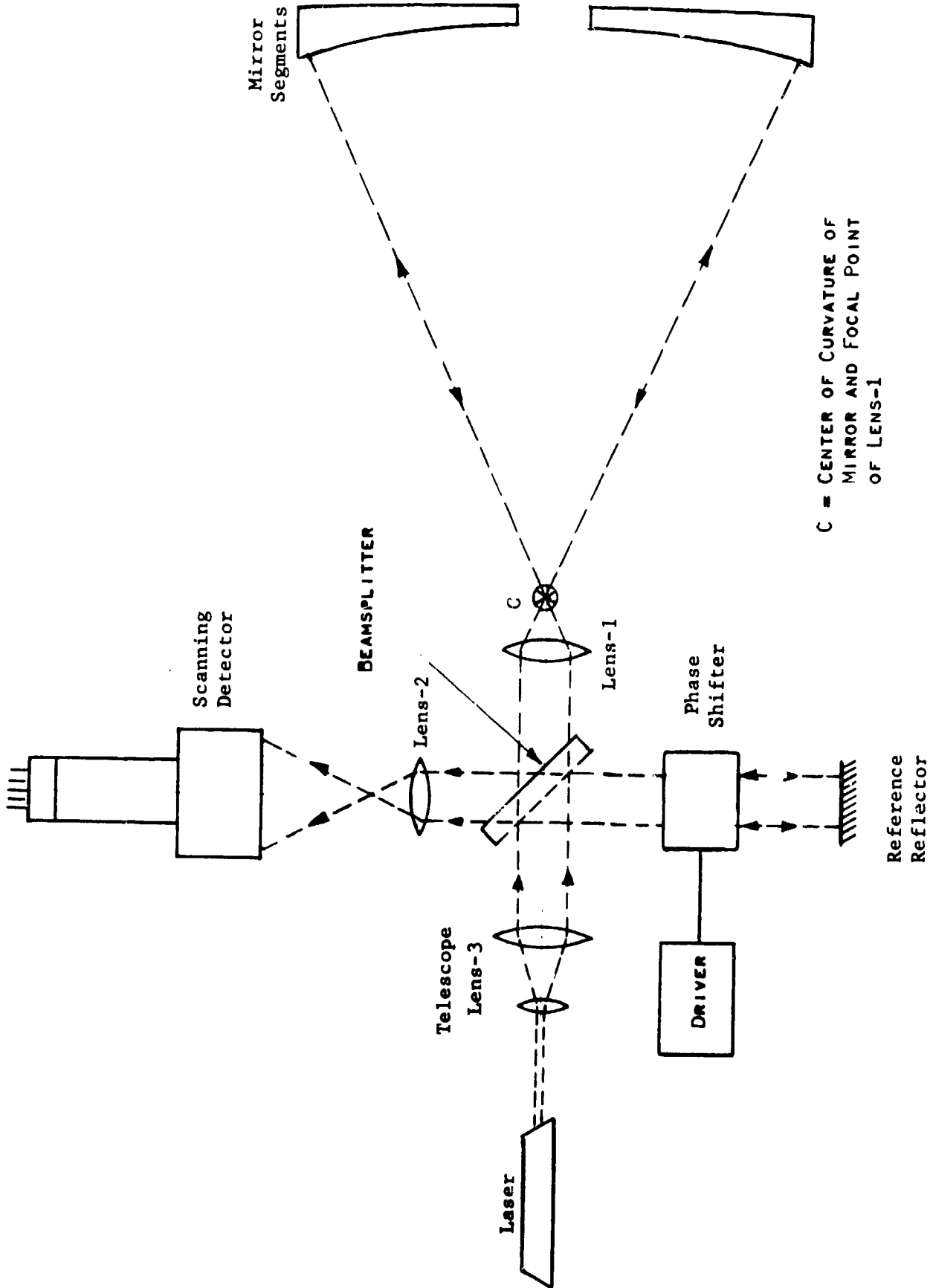
Figure 7. Phase-Measuring Interferometer Arrangement

C = CENTER OF CURVATURE OF MIRROR AND FOCAL POINT OF LENS-1

In the event of a figure error for one point in the mirror, the electronic
signal produced by a detector at the corresponding spot in the fringe pattern
will have a phase shift relative to the signal from any other perfectly aligned
point. Thus, figure errors may be recognized by the detection of phase shift
between two electronic signals; one, from a reference point, and one from the
point in question. The approach has two advantages; first, the error signal
has sense, that is the sign of the figure error can be recognized from the
sign of the phase error; second, an electronic phase shift can be readily
detected to an accuracy of a few degrees. A surface departure from spherical
of 1/200 wavelength produces 1/100 of a fringe, which in turn results in a
3-1/2° phase shift which is well within the sensitivity of an ordinary electronic
phase detector.

The components used to implement the phase measuring interferometer
are shown in Figure 8. These parts are of standard type. The only unconven-
tional element in this arrangement is the phase shifter in the reference arm.
Other elements in the interferometer include lens-1 which is used to convert
one parallel beam to a spherical converging beam with a center of curvature
"C '. Lens-2 focuses the mirror segments upon the scanning detector, permitting
a fine-grain exploration of the fringe pattern corresponding to each spot on
the mirror segment. Lens-3 is used to expand the laser beam to a practical
working size.

The performance of the phase measuring interferometer by itself
was documented in the Phase I report. The following will indicate the per-
formance as measured in the final Active Optics assembly. Figure 9 shows
typical electronic waveforms obtained by looking at two spots in the fringe
pattern simultaneously. The relative phase of the two wave forms is approximately
30° corresponding to 1/12 fringe or 1/24 wavelength departure from a spherical
shell between the two points. It will also be noted that there is a small
random phase and amplitude fluctuation. This fluctuation is caused by photon
noise in the scanner signal and perhaps a small amount of air turbulence in
the portions of the beam outside the vacuum tank. At this test point, both
signals have been integrated by a 60 cps filter with a bandwidth of 45 cps.

Figure 10 is a typical recording of interferometer accuracy. These
are records of radial figure error of the interferometer only, taken with a
small plane mirror replacing lens-1 and the segmented mirror. Shown is the
DC voltage out of the phase detector for a reference spot at the center of the
beam and a scanning spot traveling along a radius. The perturbations are
larger than desirable and were found to be due primarily to the beamsplitter.
Figure 11 shows a typical short-term stability for a measurement between two
spots in the figure pattern. It will be seen that the noise level is well
below that which is tolerable. Table I summarizes the performance of the
phase measuring interferometer as a figure sensor. In this case, one wave-
length is 0.6328 micron or 24 microinches of surface departure from design
surface.
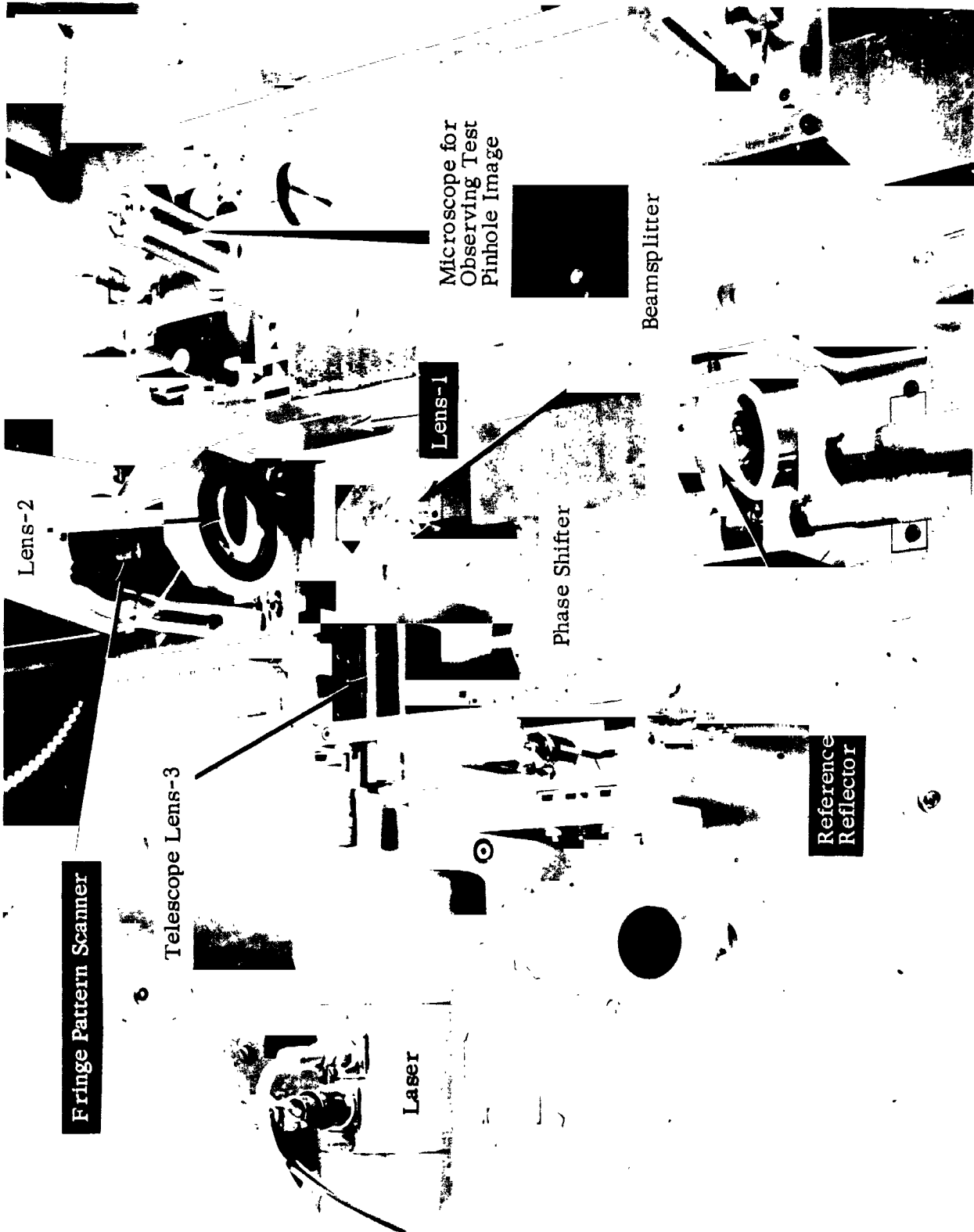
Figure 8. Phase-Measuring Interferometer
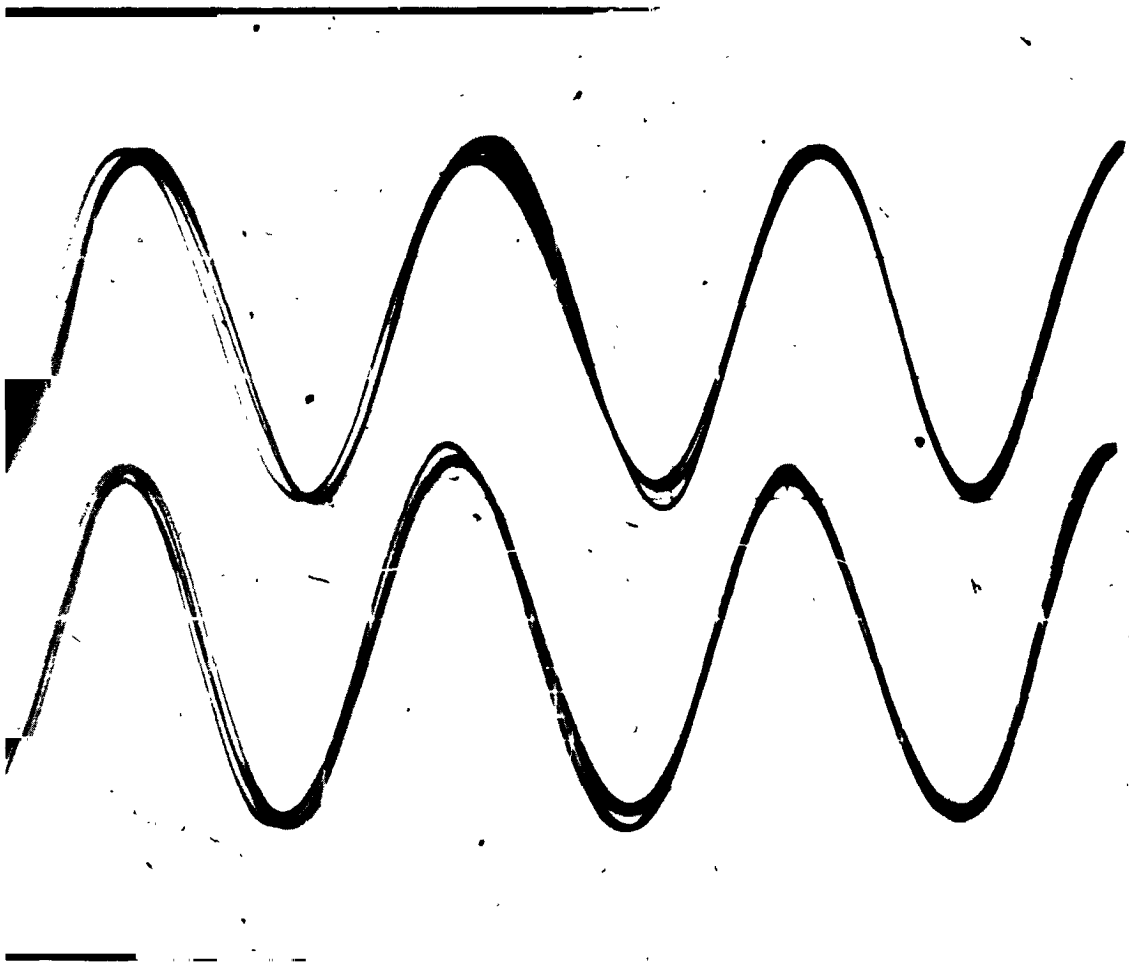
60 CPS signals from two spots on the mirror after filtering showing
approximately 30° phase difference and some random fluctuations in
phase and amplitude due to photon noise.

Figure 9.   Phase-Measuring Interferometer Waveforms
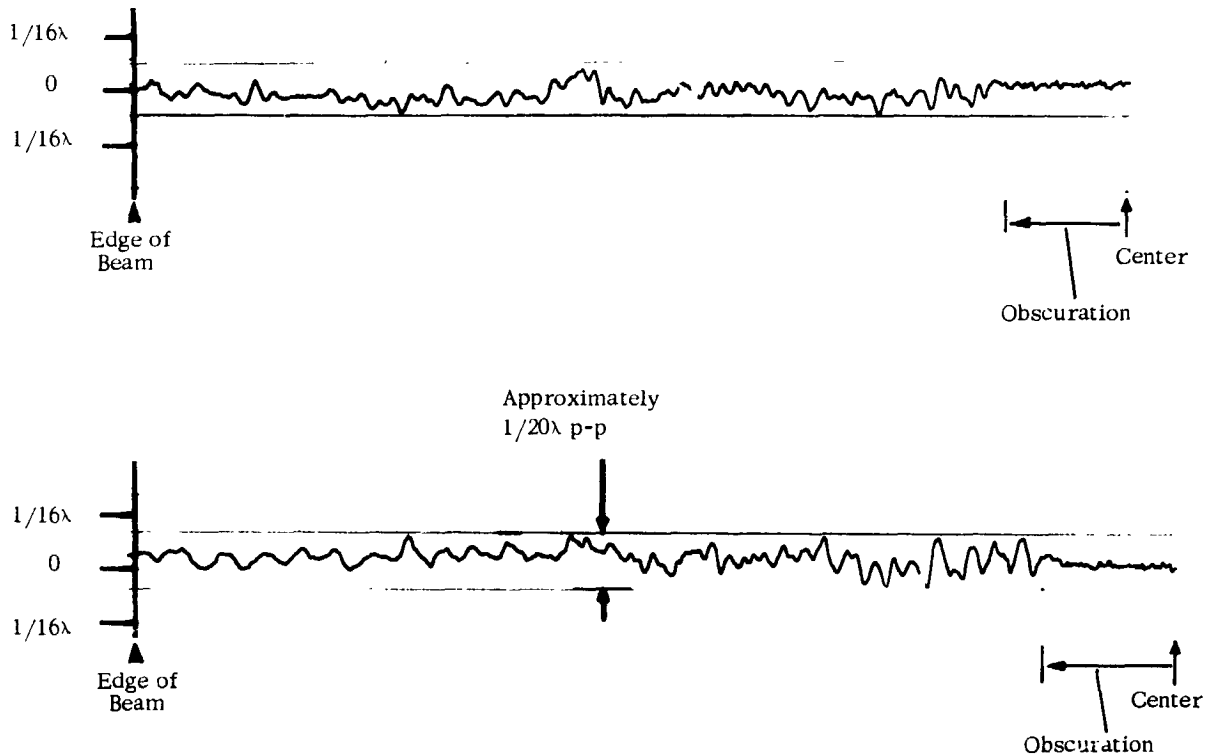
Showing figure error for two radial scans of interferometer
using a small plane mirror with center obscuration in place
of lens-1 and segmented mirror.

Figure 10.   Typical Accuracy Recording For
Phase-Measuring Interferometer

1/32 Wave Equivalent
Surface Deformation

10 Seconds
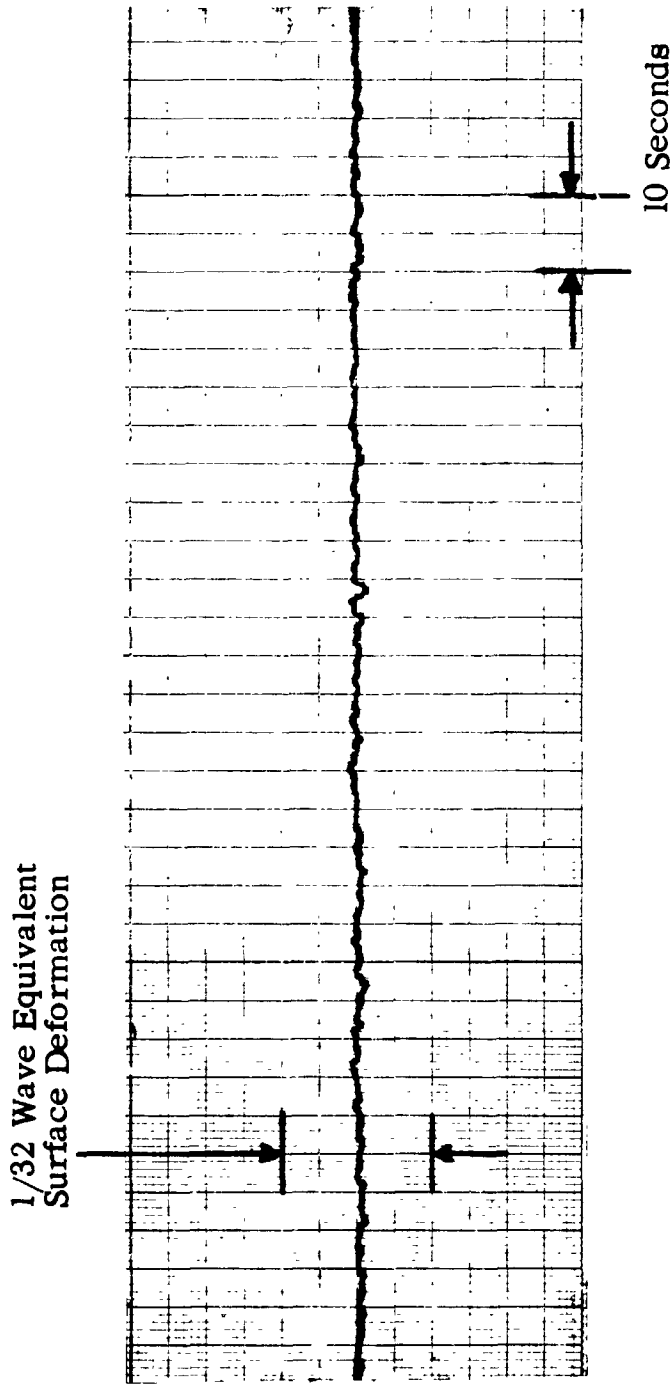
Illustrating the random fluctuations of phase detector output
for steady state comparison between two points in fringe
pattern with a flat mirror in place of segmented mirror.

Figure 11.   Typical Stability Recording Phase-Measuring Interferometer

TABLE I

PHASE MEASURING INTERFEROMETER PERFORMANCE

	DESIRED	ACHIEVED
Static Accuracy	< 1/20 λ p-p	1/20 λ p-p
Short Term Stability	<< 1/20 λ rms	~ 1/1000 λ rms
Long Term Stability	< 1/25 λ /sec	1/45 λ/hr
Total Range (Max. recognizable tilt)	200 λ	~ 50λ
Unambiguous Range	10μ in.	10μ in.
Response Time	10 channels per 1/2 sec	11 channels with 0.1 sec time constant

3.2.2 Ambiguity Sensor

The fine figure sensor employs coherent light as the illuminating source with the result that it is impossible to recognize relative displacements of integral 1/2 wavelength. The ambiguity sensor resolves this uncertainty, and generates a control signal for positioning the segments within ±5 micro-inches of each other. The approach selected employs an equal-path interfero-meter located immediately above the gap between the two segments so that one beam is reflected from the surface of each segment. A white light source is used so that good interference occurs only when the two paths are equal, that is, when both segments are the same distance away from the interferometer.

In principle, this is the inverse of the Michaelson interferometer spectrometer, in which the interferogram generated by varying the relative path length in a two-beam interferometer is analyzed to determine the spectral content, of the excitation energy. In this application, a wide-band excitation source and detector are used so that the zero order interference lobe is readily recognizable from any other order. Thus, it is possible to sense when the two segments are co-planar within a fraction of a wavelength. The implementa-tion of the white light interferometer is shown in Figure 12. A Koesters prism performs the function of beamsplitting and re-combination. Wide spectral response is obtained by using a tungsten arc source and lead sulphide detector. A simple vibrating fork chopper modulates the light so that AC detection may be used in the electronics. A typical interferogram generated by translating one segment relative to another is shown in the bottom trace of Figure 13. The peak, or zero path difference point, is easily distinguished from the other
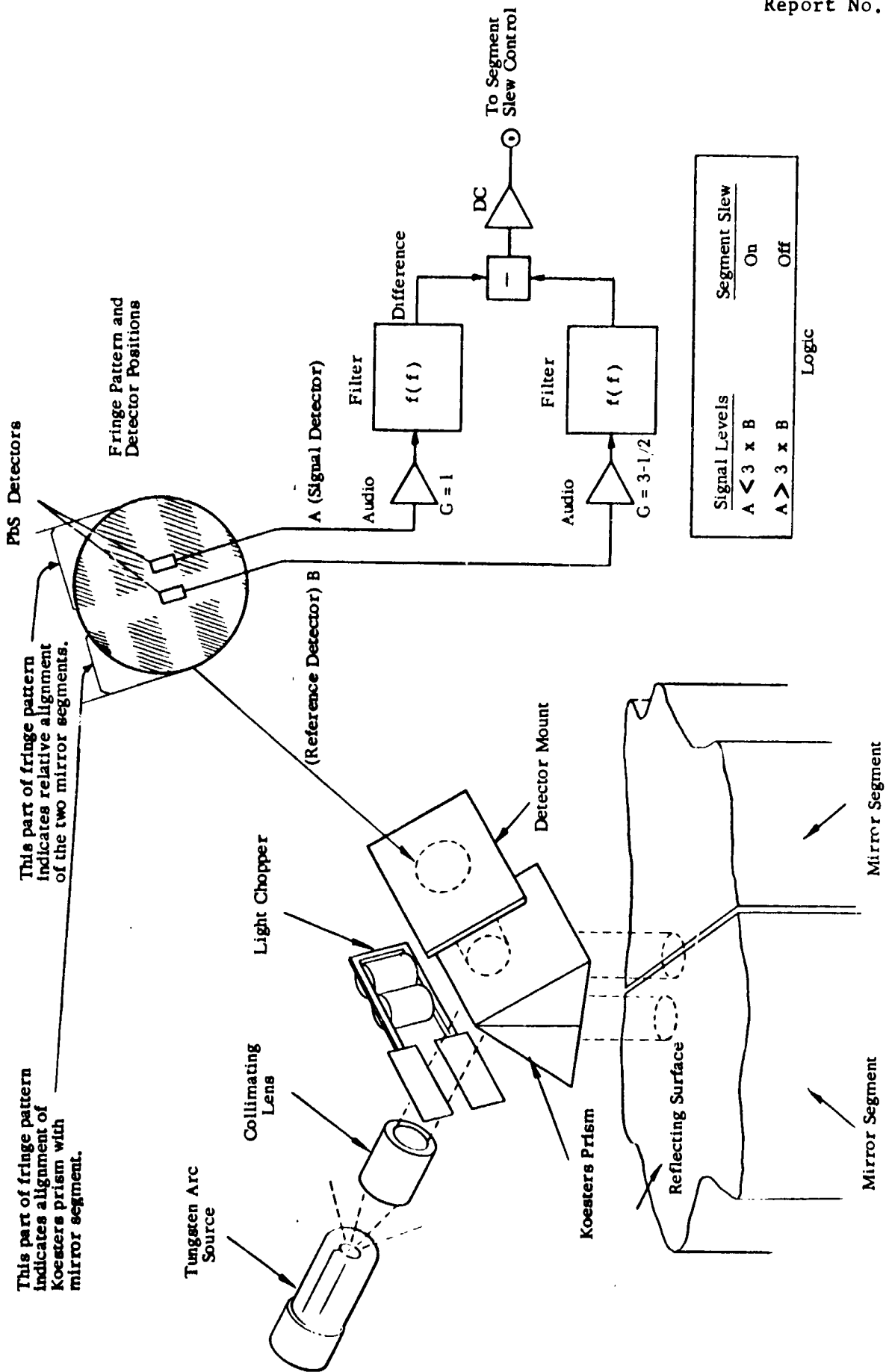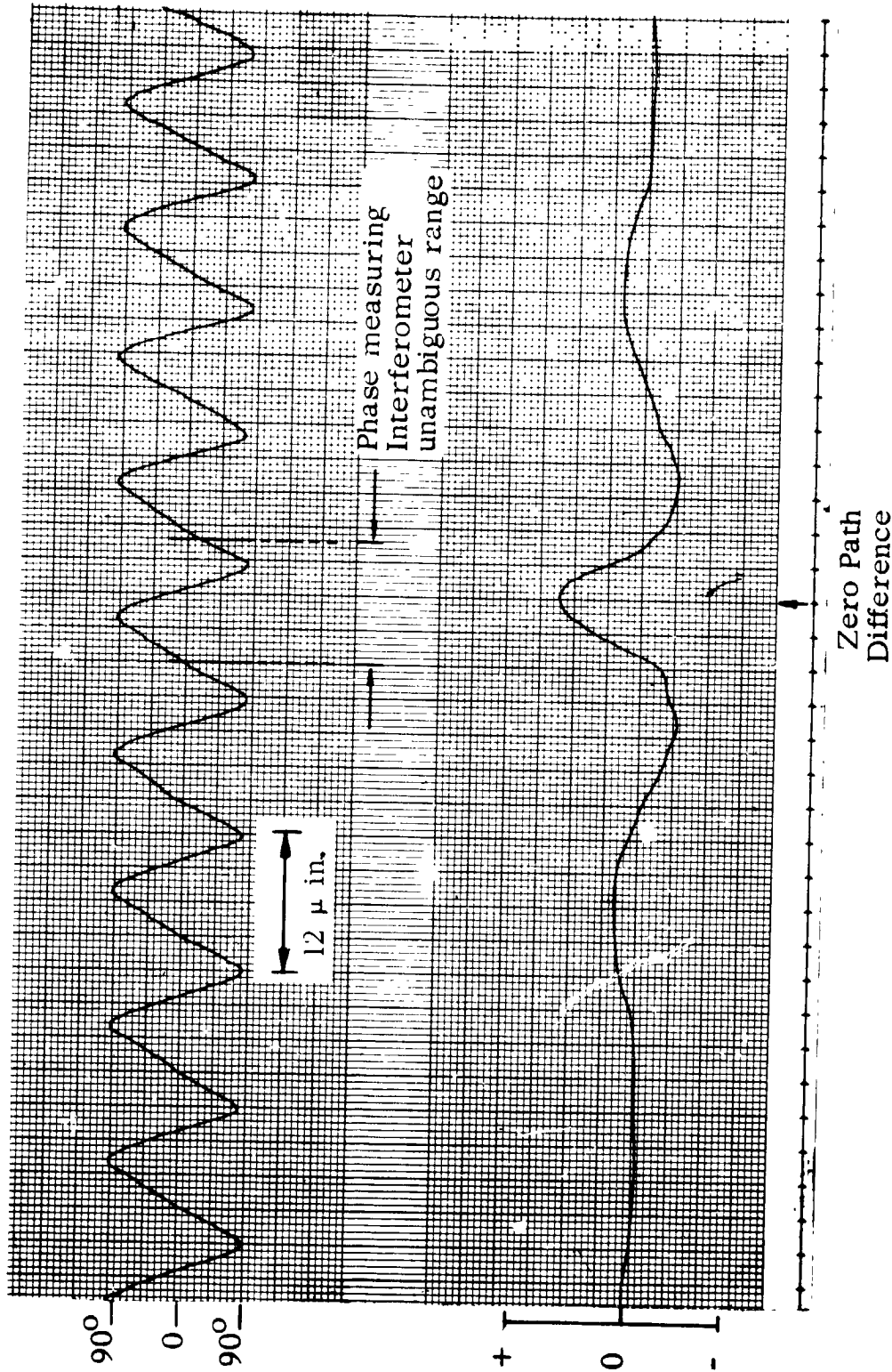
Figure 12. White Light Interferometer Arrangement

21

Figure 13. White Light Interferometer Interferogram

Showing difference between fringe signal and reference signal as Segment II is moved axially relative to Segment I.

22

orders of interference. The top line of Figure 13 is a calibration of rela-
tive displacement between the two segments as indicated by the phase measuring
interferometer. It can be seen that the white light interference peak occurs
at the cross-over point, or point of zero phase difference as indicated by the
phase measuring interferometer; and that the width of the peak is within the
unambiguous range of the figure sensor. Figure 14 shows the white light in-
terferometer components mounted above the intersection of two segments. Fig-
ure 15 shows the fringe pattern generated by this interferometer for a slight
amount of tilt in the prism. This is incorporated to facilitate alignment of
the prism. Also shown is a second detector in the center of the pattern at
a spot corresponding to the gap between the two segments. This detector re-
ceives light from one beam only, and its output is used as a reference level
in the electronics to minimize the effect of variation in the tungsten arc
source output.

The performance of the white light interferometer was measured
during Phase I. The results are repeated in Figure 16. This is a graph of
the relative displacement between two small mirrors as controlled by the
signal from the white light interferometer. The experimental procedure con-
sisted of translating one mirror position relative to the other through the
equal path point and using the signal generated by the white light inter-
ferometer zero order interference lobe to stop the translation. This proce-
dure was repeated many times in both directions with the result as shown.
During the time the data was being collected, a drift occurred in the center
of the stop band due to thermal effects in the mounting arrangement. The stop
band followed the drift correctly with a width well within the 10 microinch
unambiguous range of the phase measuring interferometer.

3.2.3 Coarse Tilt Alignment

The problem of coarse tilt alignment was not investigated exten-
sively because it was believed to be less significant. There are at least
two signatures which can be used, the best being the position of the return
beam in the phase measuring interferometer relative to the point C in a plane
perpendicular to the optical axis. If a segment is oriented so that its center
of curvature is a radial distance r away from the focal point of lens-1, i.e.,
point "C" in Figure 7, then the return beam will come to focus a distance 2r
away from point "C" in the same radial direction. Figure 17, shows a scheme
for detecting this displacement. A four-facet prism with a central hole is
located with its apex at point "C." Four lenses, one for each facet of the
prism, focus the mirror on four detector arrays. Each detector array has
the same number and shape detectors as segments in the mirror. In the pres-
ence of coarse tilt misalignment, the return laser beam falls on one of the
facets of the prism. A lens then images the out of tilt segment on its corres-
ponding detector in the detector array which is opposite the reflecting facet.
Thus, unambiguous up-down, or left-right control signals can be generated for
each segment. If the center hole is 0.04 inch in diameter, this scheme will
provide error signals well within the point where 100 fringes are produced by
the phase measuring interferometer.

Showing Koesters prism mounted to one mirror segment; light
source, chopper, and detector mounted to support frame.

Figure 14.   White Light Interferometer

Two patterns are shown; one pattern from segment the prism
is mounted on, and one from interference between two adja-
cent segments; dark zone in center is reference light from
one beam of interferometer only.

Figure 15. White Light Interferometer Fringe Pattern

Figure 16. White Light Interferometer Performance
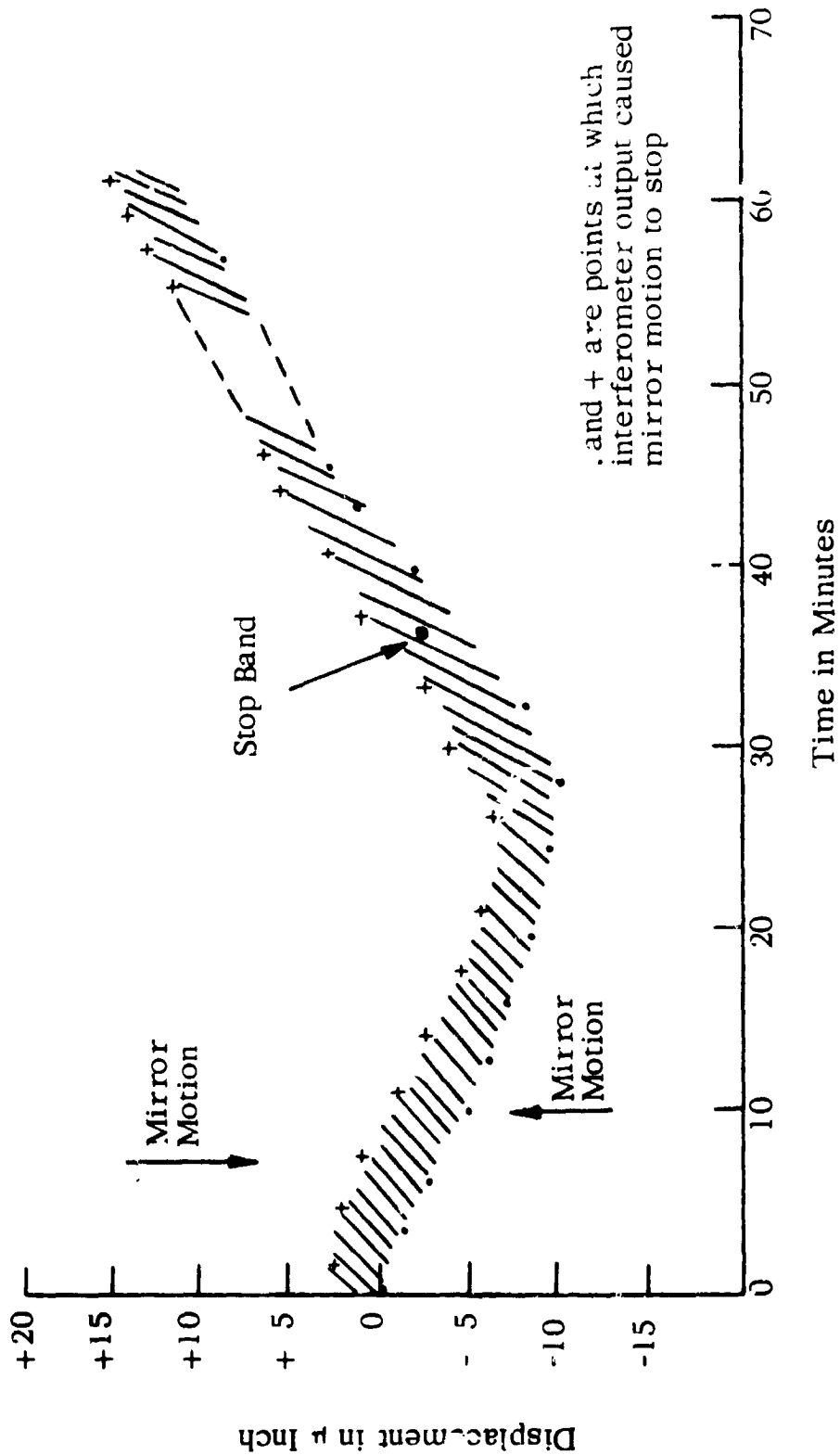
Showing the relative positions at which slew of one segment relative to second was stopped by signal from white light interferometer. Long term drift was due to thermal drift in mount.

. and + are points at which interferometer output caused mirror motion to stop
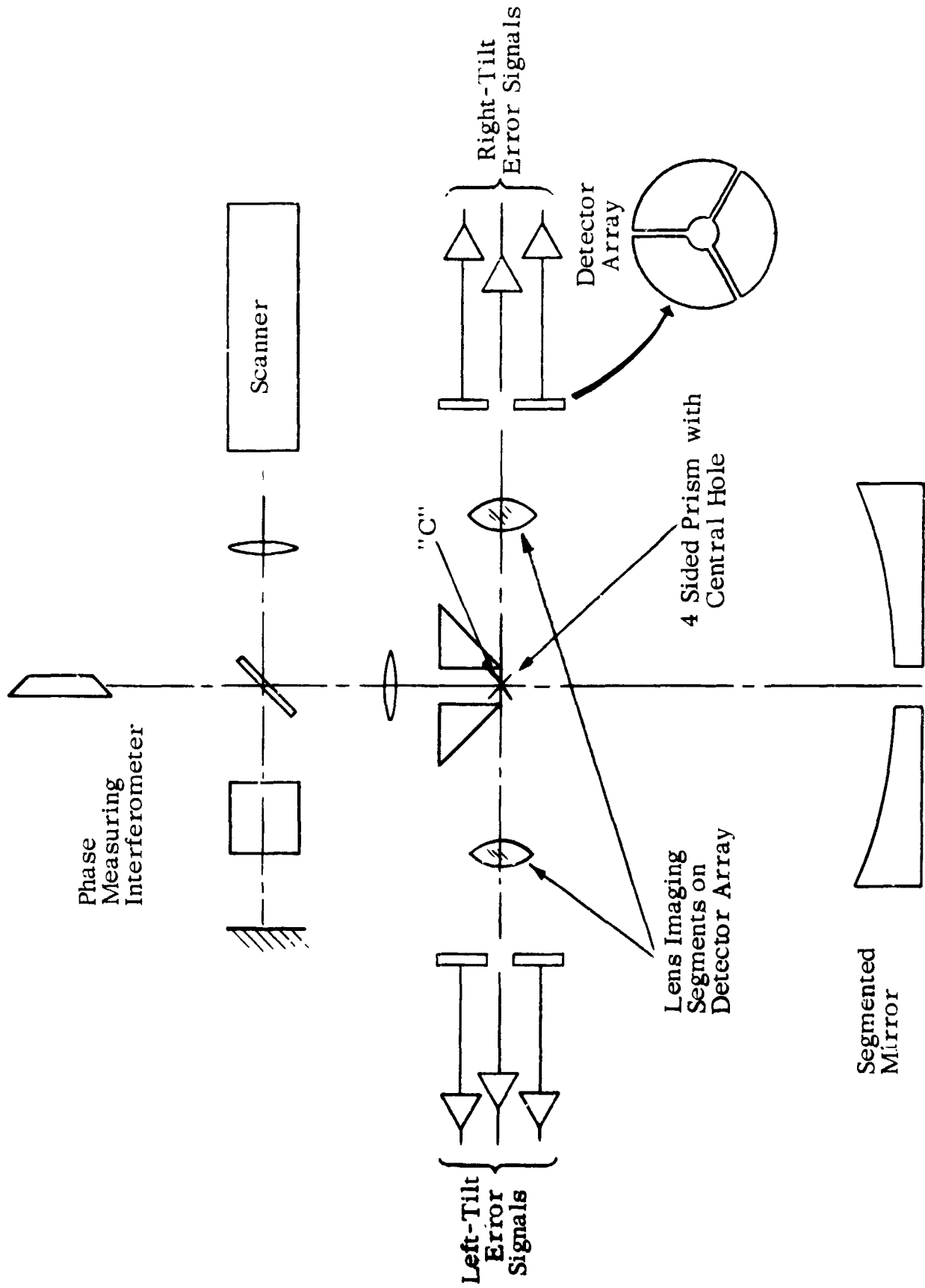
Figure 17. Coarse Tilt Alignment Concept. For tilt misalignment greater than 100 fringes

3.2.4 Image Scanner

It is necessary to monitor a large number of points in the inter-
ferometer fringe pattern, either simultaneously, or in quick succession.
Several different types of image scanning devices were evaluated during the
Phase I investigation. An image dissector camera was selected as most appro-
priate because it provided the desired resolution, spectral response, and
frequency response. Because the fringe pattern is intensity modulated at a
60 cycle per second rate, it was not possible to use an integrating image
scanner such as a vidicon camera. A commercial image dissector camera manu-
factured by ITT was purchased. The unit used for the experiment has a 1-1/2
inch diameter tube with 1-1/2 mil scanning aperture, and an S-11 photocathode
surface. Experience gained during the course of the project indicates that a
better choice would be an S-20 surface and a 5-mil scanning aperture. Table
II shows the characteristics of the camera used for the demonstration; Figure
18 shows the actual camera.

The alignment sequence required both a scanning spot and sequential
sampling of a number of fixed spots. The scan pattern is shown in Figure 19.
Points 1, 4, and 7 are reference spots for segments I, II, and III respectively.
Scans go from 1 to 2 and 1 to 3 for tilt alignment, and from 1 to 10 for axial
alignment of segment I. Similar scans are required for segments II and III.
The electronics also provided the facility for a manual positioning of a
roving spot anywhere within the beam. Figure 20 shows the scanner deflection
waveforms for X and Y deflection. The clock rate of this scan was 3300 cps
and the frame rate 300 fps; that is, eleven spots were scanned sequentially,
300 times per second.

The image dissector scanner tube is essentially a scanning photo-
multiplier. There is no integration at the photocathode; hence, the output
current will show the evidence of photon noise. The bottom trace of Figure 21
shows the output signal of the image dissector camera with evidence of photon
noise. At this point, the signal has passed through a video amplifier with
a bandwidth of over 1 megacycle.

3.3 **CONTROL ELECTRONICS**

A variety of functions are provided in the control electronics con-
sole including:

- Manual Sequencing Control
- Scan Waveform Generation
- Signal Decommutation and Filtering
- Phase Detection
- Signal Differential Detection
- Servo Amplification

Figure 18.   Image Dissector Camera

Figure 19 . Scan Pattern
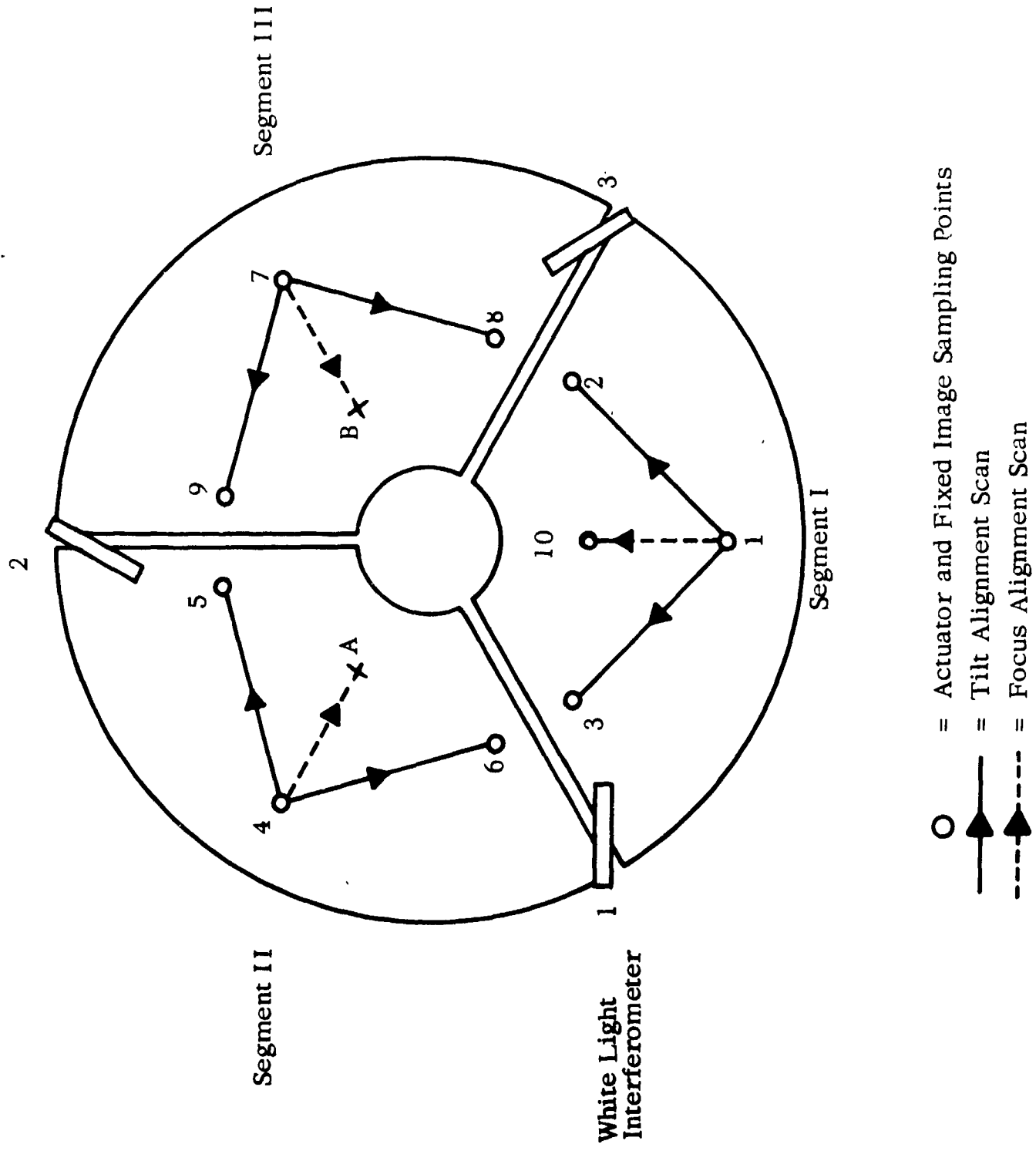
○ = Actuator and Fixed Image Sampling Points
━━▲ = Tilt Alignment Scan
╌╌▲ = Focus Alignment Scan
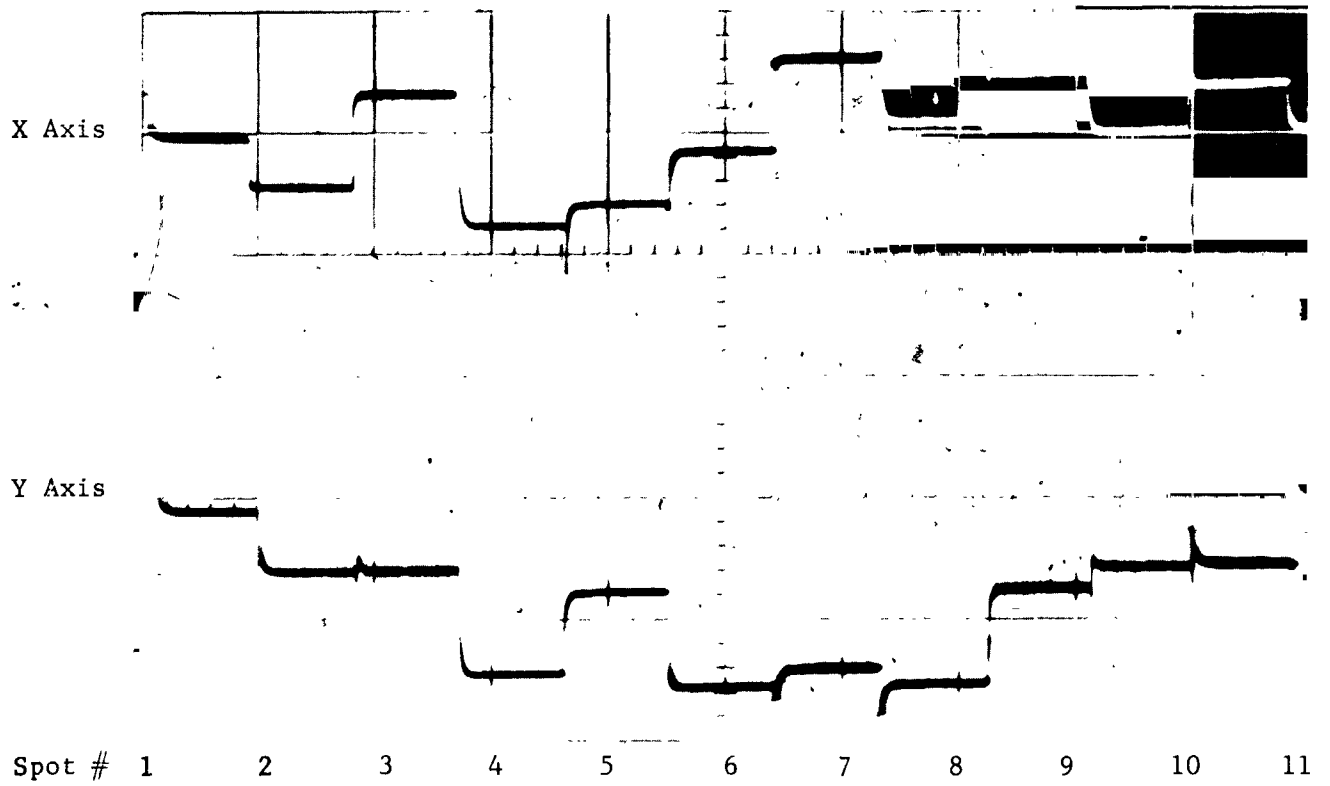
Showing X and Y deflection voltages versus time for one frame of scan spot multiplexed through 11 positions.

Figure 20. Scanner Deflection Waveforms
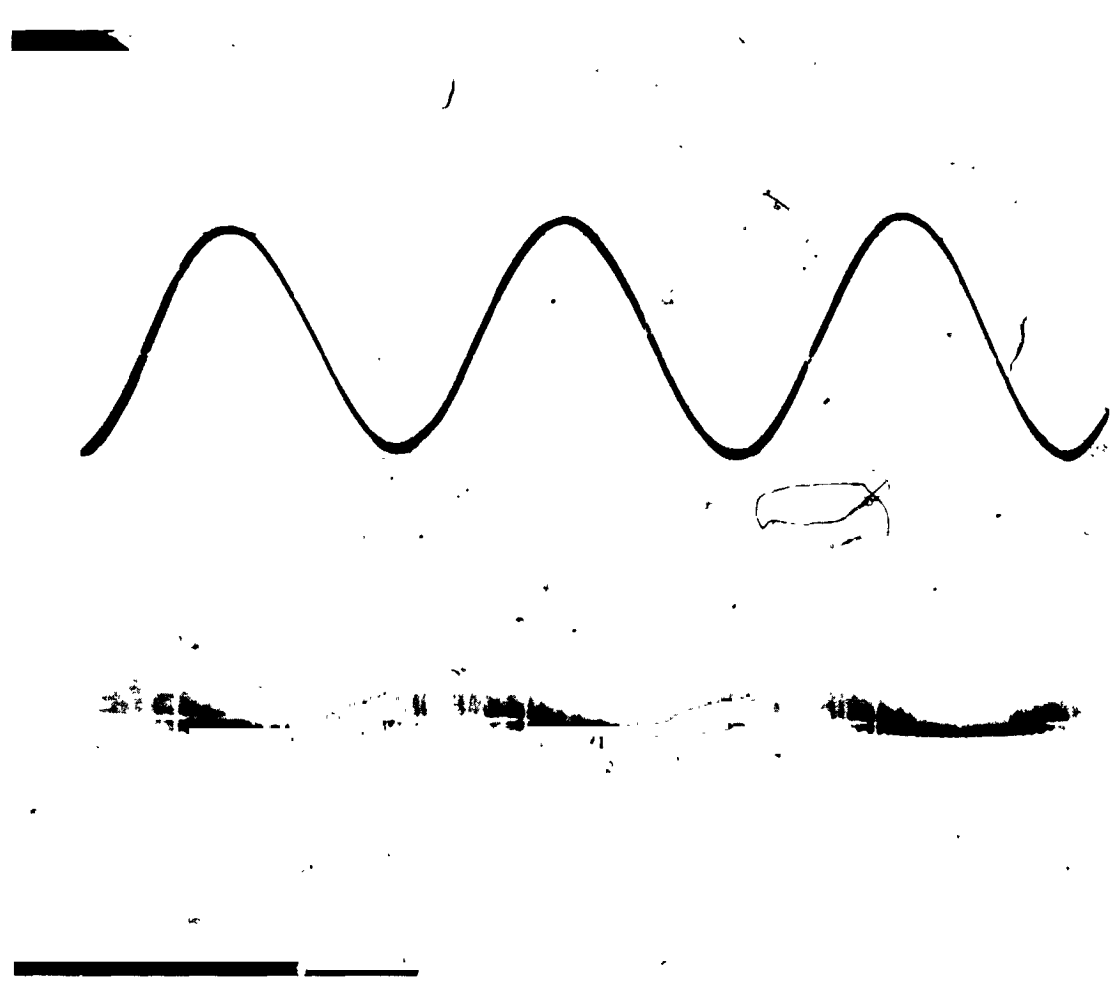
Top trace is a 60 cps reference waveform. Bottom trace is
scanner output before filtering when looking at one spot
only showing effect of photon noise.

Figure 21. Image Dissector Signal

TABLE II

IMAGE SCANNING CAMERA
SPECIFICATIONS

Tube Type:	Image dissector, 1-1/2-inch diameter, 1-1/2 mil aperture
Resolution:	Better than 750 TV lines at 50% response
Photocathode:	S-11 Surface
Frequency Response:	Greater .an 50kc at 50% response with no ×-Y sc :n
Dynamic Range:	Greater than 100:1 . output
Video Amplifier:	5 cps to 50kc at 3 db response
Deflection Amplifiers:	dc to 10 kc, X and Y deflection
Lens:	None
Camera Head Size:	Approximately 4" x 6" x 12", portable for remote operation
Camera Control:	Separate cabinet

Manual switching from one function to the next in the alignment procedure will be described in Section 4.1 under System Performance. The scan waveforms discussed in Section 3.2.4 commutate the image dissector detection aperture between eleven spots at a frame rate of 300 frames per second. The position of ten fixed spots are selected by a set of X-Y potentiometers. The scan spot can be programmed to go between any two selected fixed spots. The potentiometers are sampled sequentially by a clock-driven logic network. The same logic is used to decommutate the scanner output signal to eleven channels in which eleven separate 60 cps carriers are generated, one corresponding to each of the eleven spots on the mirror. Figure 22 shows the decommutated waveform before and after filtering. The bottom trace shows the boxcar output immediately after the commutation while the top trace shows the result of filtering by a 45 cps bandwidth filter.

The various signals from the decommutator are selected in accordance with the function desired and fed to a set of ten phase detectors. For example, when aligning in tilt about the 1-3 axis in segment I, the dissector scan goes from spot 1 to spot 2 and signals are selected from spot 1 and a moving scan spot, identified as spot 11. These signals are compared in a phase detector and the resulting DC error signal is used to drive actuator 2 in a direction to reduce the DC error. Thus, a tilt alignment servo loop is closed. Filter networks are incorporated between the phase detector and servo amplifier to minimize the effects of photon noise and air turbulence, and to insure that the closed loop operation will be stable. The servo amplifier uses rate feedback from a tachometer on the servo motor to stabilize the motor control minor loop.

The circuit schematics used for the foregoing functions are quite standard and will not be included. Figure 23 shows the electronic console with its many control switches.

3.4 ACTUATORS

An actuator which can provide the actual mechanical displacements required, with the necessary precision, range, efficiency and reliability is a key element in the development of an active positioning system. Several candidate actuators designs have been investigated. The most promising of these was the Peristaltic actuator (a magnetostrictive model of this actuator was described in the Phase I Report). However, it was found that an undue amount of development would have been required if this were to be used. Therefore, for this project a differential spring actuator was selected which provides the precise motion desired (less than 1/2 microinch) and has an adequate range (±0.010 inch). A photograph of the actuator components and a diagram of the assembly are shown in Figures 24 and 25.

In operation, an error signal generated by the phase measurement interferometer is used to develop a rotation of the servo motor in the appropriate actuator. The servo motor has a gear train which reduces the motion applied to the lead screw by a factor of 227:1. The lead screw, therefore, turns once for 227 turns of the servo motor. The lead screw advances a nut
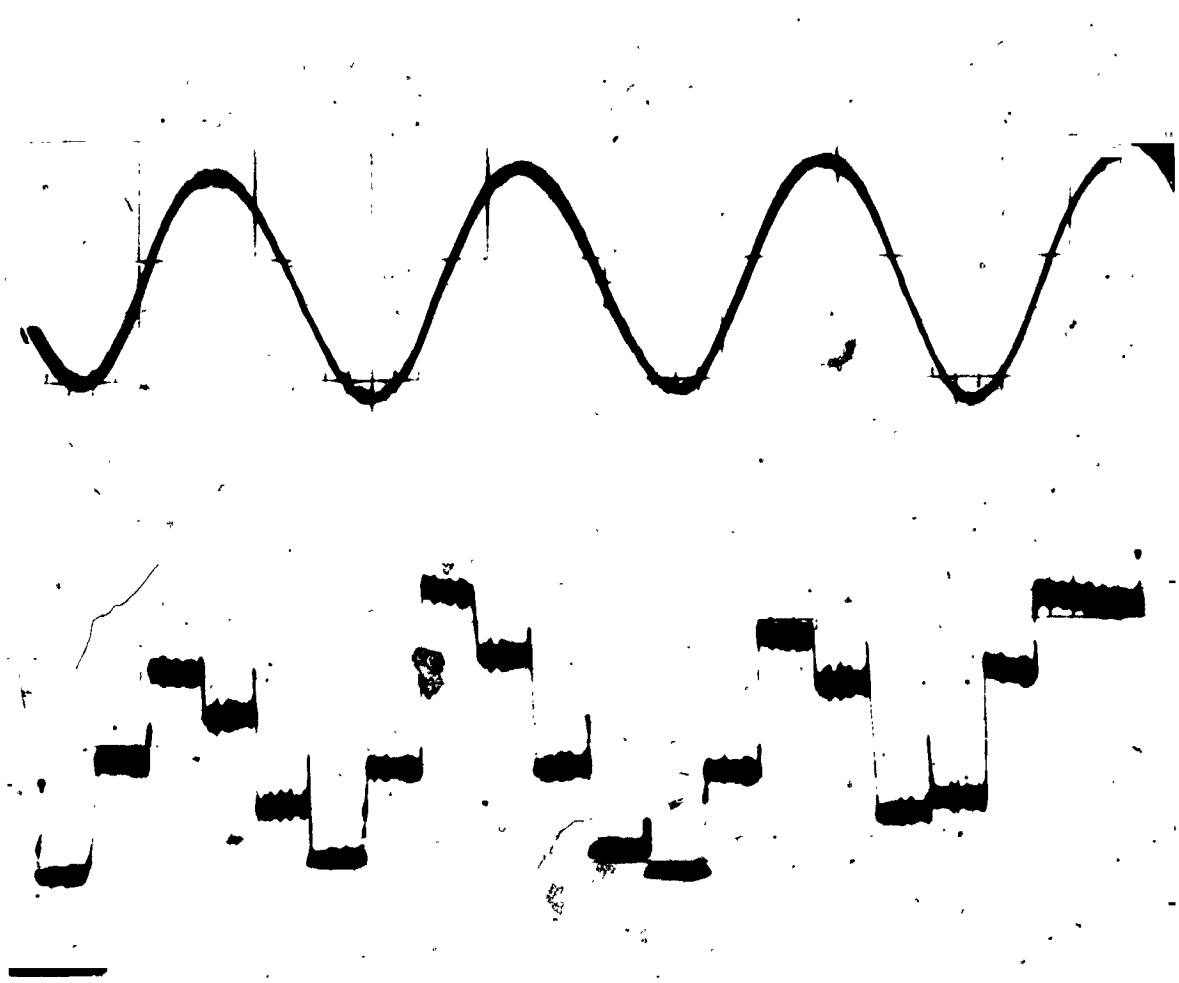
Top trace is a 60 cps reference. Bottom trace is a demultiplex
output before filtering, showing effect of "box-car" clamp.

Figure 22. Demodulator Waveforms
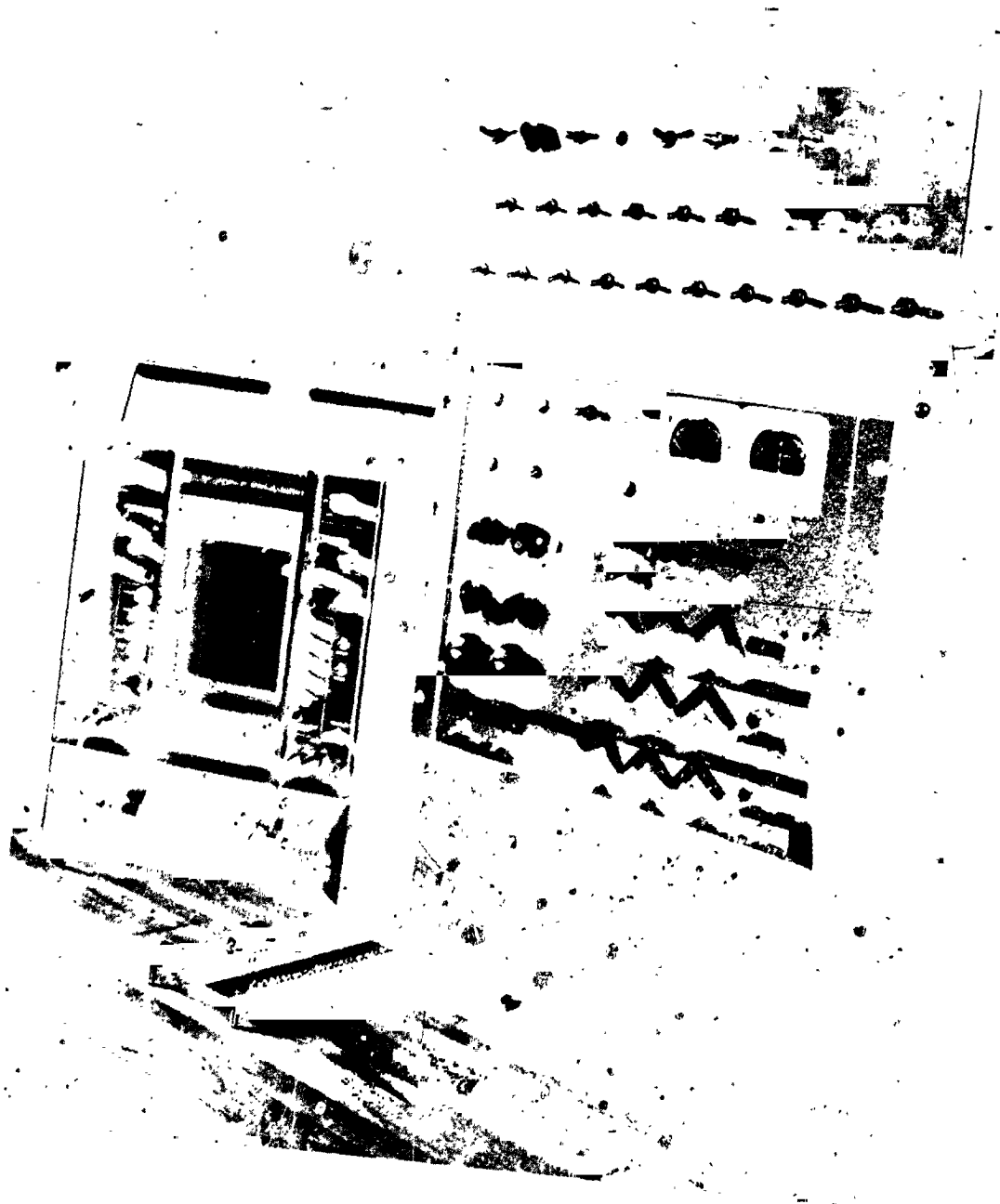
Showing control switches for manually selecting the various
automatic functions for the nine actuators; a portion of the
vacuum tank with its thermal insulation is shown in the
background.

Figure 23. Electronics Console

Figure 24. Actuator Assembly Diagram

Figure 25. Actuator Parts (Spring Damping not Shown)

End Plate

Mounting Flange

Stiff Springs
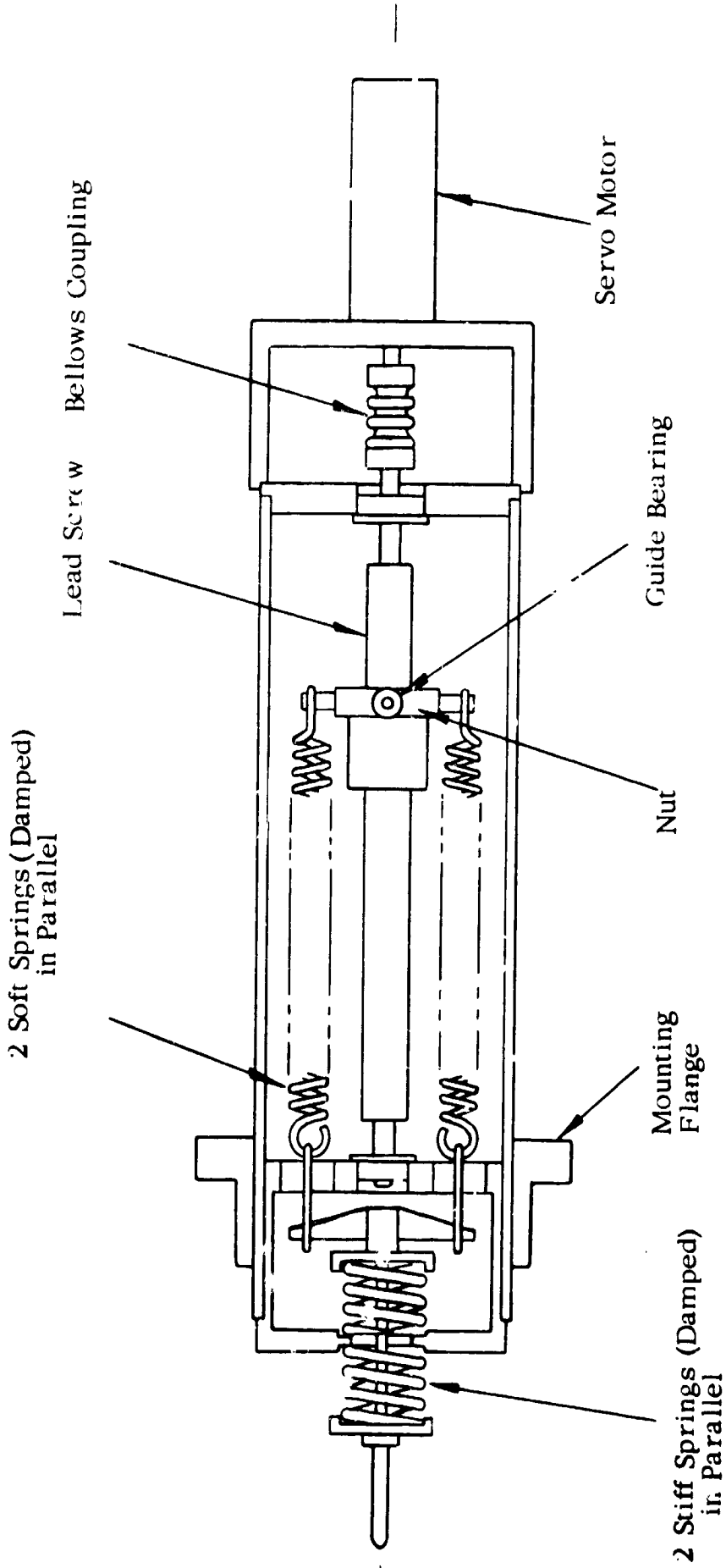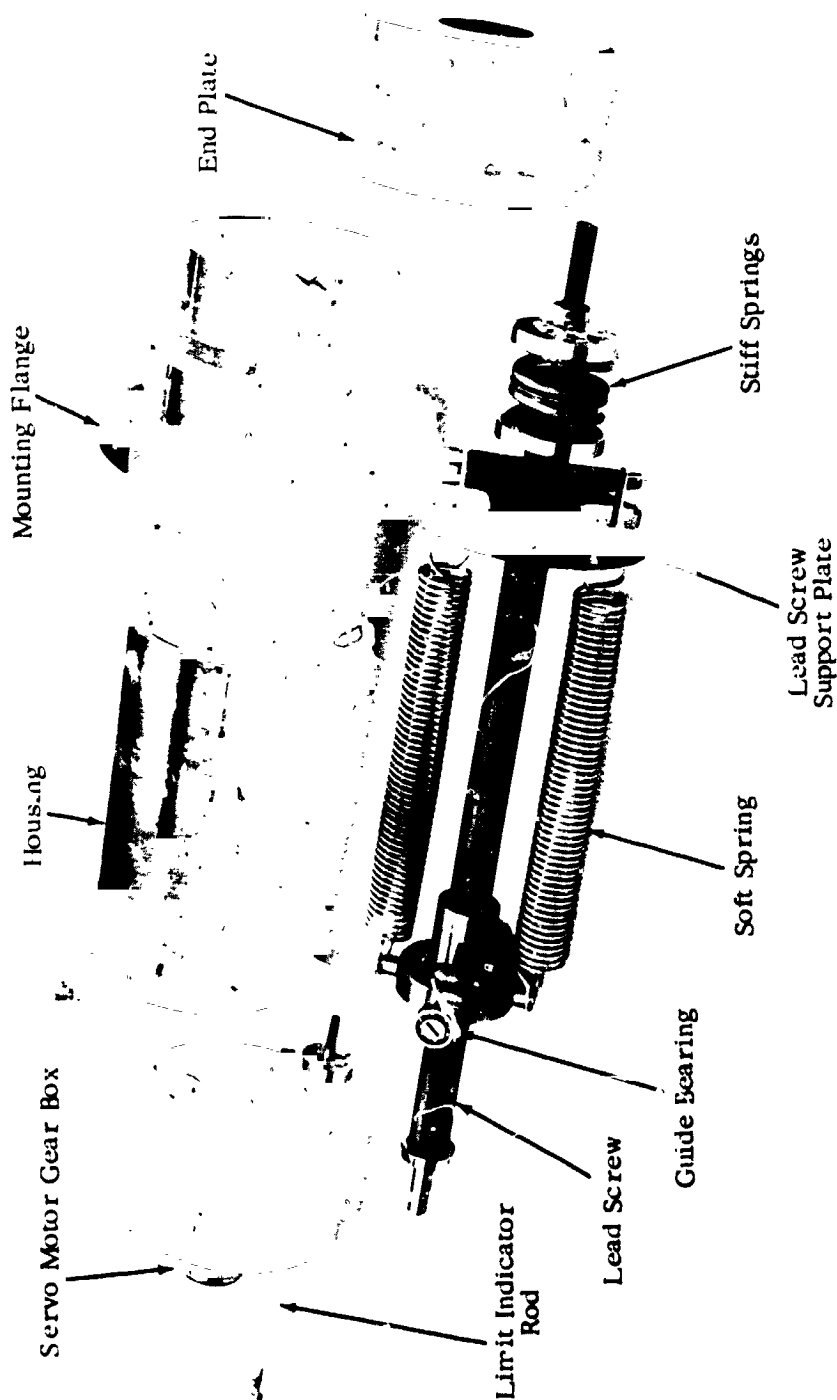
Housing

Lead Screw
Support Plate

Servo Motor Gear Box

Soft Spring

Limit Indicator
Rod

Lead Screw

Guide Bearing

which varies the extension of the soft springs which pull against the stiff springs. The stiff springs are displaced 1/160 of the deformation of the soft springs. A change in dimension of the stiff springs results in a change in position of the mirror segment against which the actuator is located. A single turn of the lead screw changes the ex ension of the soft springs by 0.025 inch which results in a motion of the mirror segment of approximately 160 microinches. This means that one turn of the servo motor results in a mirror displacement of approximately 1/2 microinch.

The open loop response of two typical differential spring actuators to a square wave voltage applied at the servo amplifier input is shown in Figure 26. A small time delay is evident between the time that voltage is applied and the actuator responds. This lag is equivalent to a backlash of less than 1/2 microinch in most cases. Actuator 4 shows a slight hysteresis which had no observable adverse effects on the closed loop operation. Backlash and friction effects in this type of actuator are primarily restricted to the mechanism between the servo motor and the soft springs and are transmitted to the mirror reduced by a factor of at least 160, i.e., the ratio of the soft and stiff spring constants.

A disadvantage of this actuator is its susceptibility to vibration because of its spring constants. The stiff springs used here have a constant of 600 lbs/in., which together with the mass of the segment gives a resonant frequency of approximately 30 cycles per second. This is not excited by the servo system but can respond to transients. Damping has been applied to the springs with some success to reduce the effects of vibrations. Figure 27 shows the effect of vibration with different amounts of damping. In the first case, a small amount of damping was applied to the stiff springs. In the second case, the amount of damping on the stiff springs was increased and damping was applied to the soft springs as well. The damping has reduced the effect of vibrations of the system to an average peak-to-peak value of $\lambda/50$ in the normal operating environment of the laboratory system. Further reduction of the effects of vibration through the spring system could be obtained by scaling up the spring stiffnesses.

The actuators are equipped with limit switches which provide a warning if the dynamic range is exceeded, to prevent accidental overrun and damage to the servo motor gear trains.

3.5 MOUNTING ASSEMBLY

A horizontal mounting system was selected for the closed loop experiment to make the sensing system and mirror-actuator assembly easily accessible and to facilitate making changes, modifications, and adjustments to the system. The selection has been justified by the number of times it has been necessary to remove and replace the mirror and actuator assembly from the vacuum tank.

As shown in Figure 28 each mirror segment is supported at its center of gravity by a set of flexure bearings arranged in a universal joint.

Servo Amplifier
Input Voltage
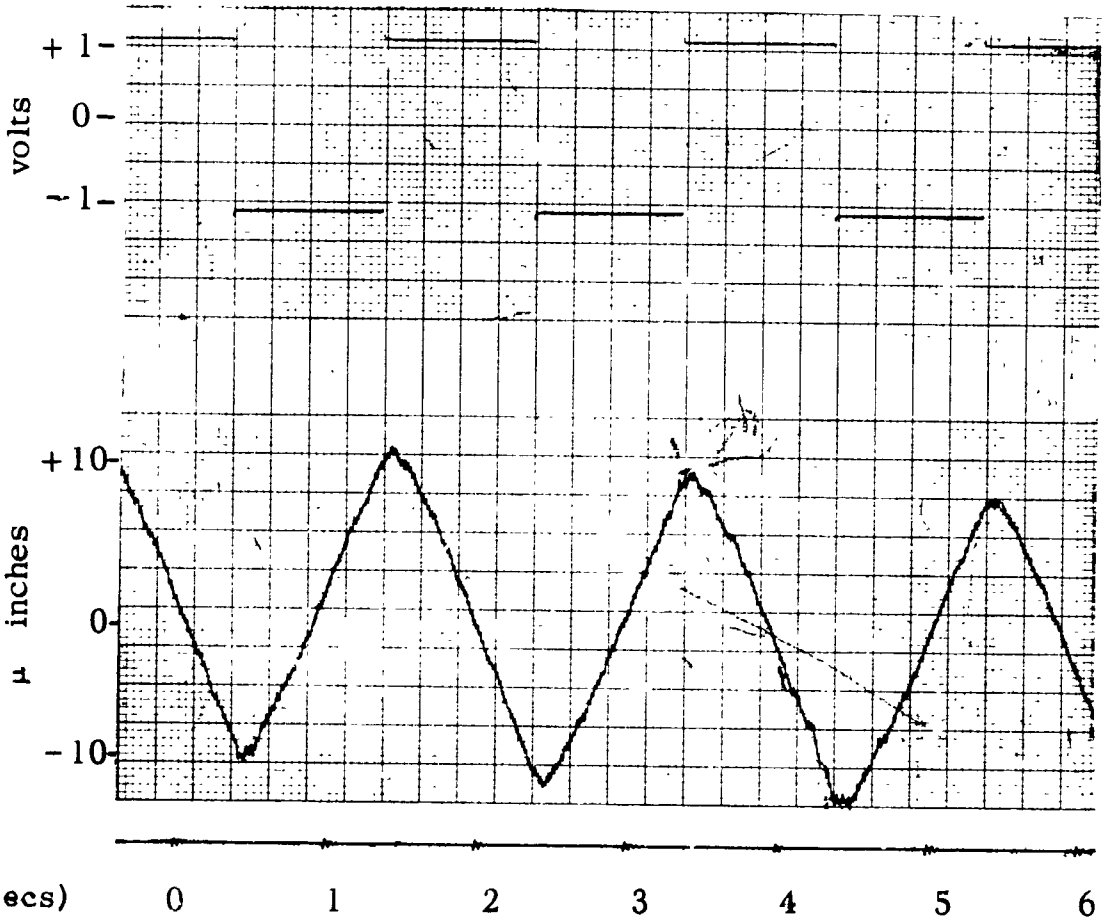
Actuator (#5 - 1)
Displacement

t(secs)

Servo Amplifier
Input Voltage
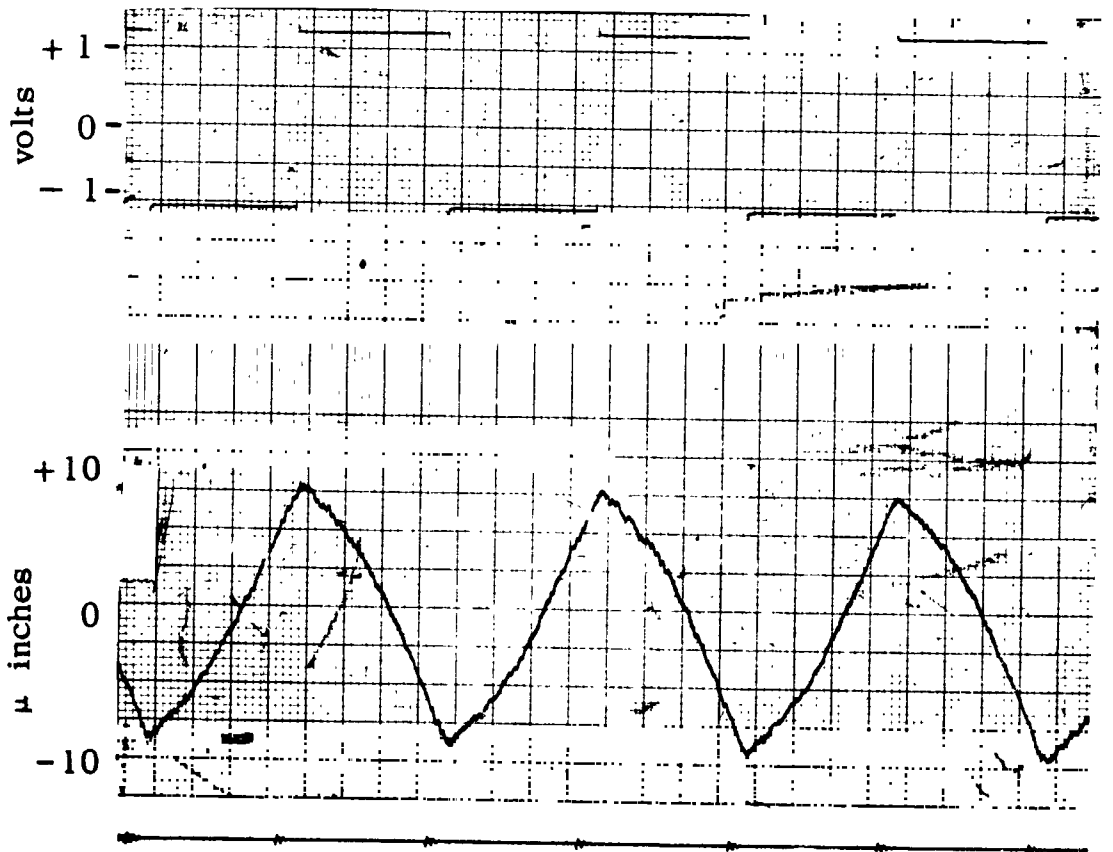
Act. .or (#9 - 66)
Displacement
(Showing Slight
Hysteresis)

Figure 26. Typical Performance Differential Spring Actuators
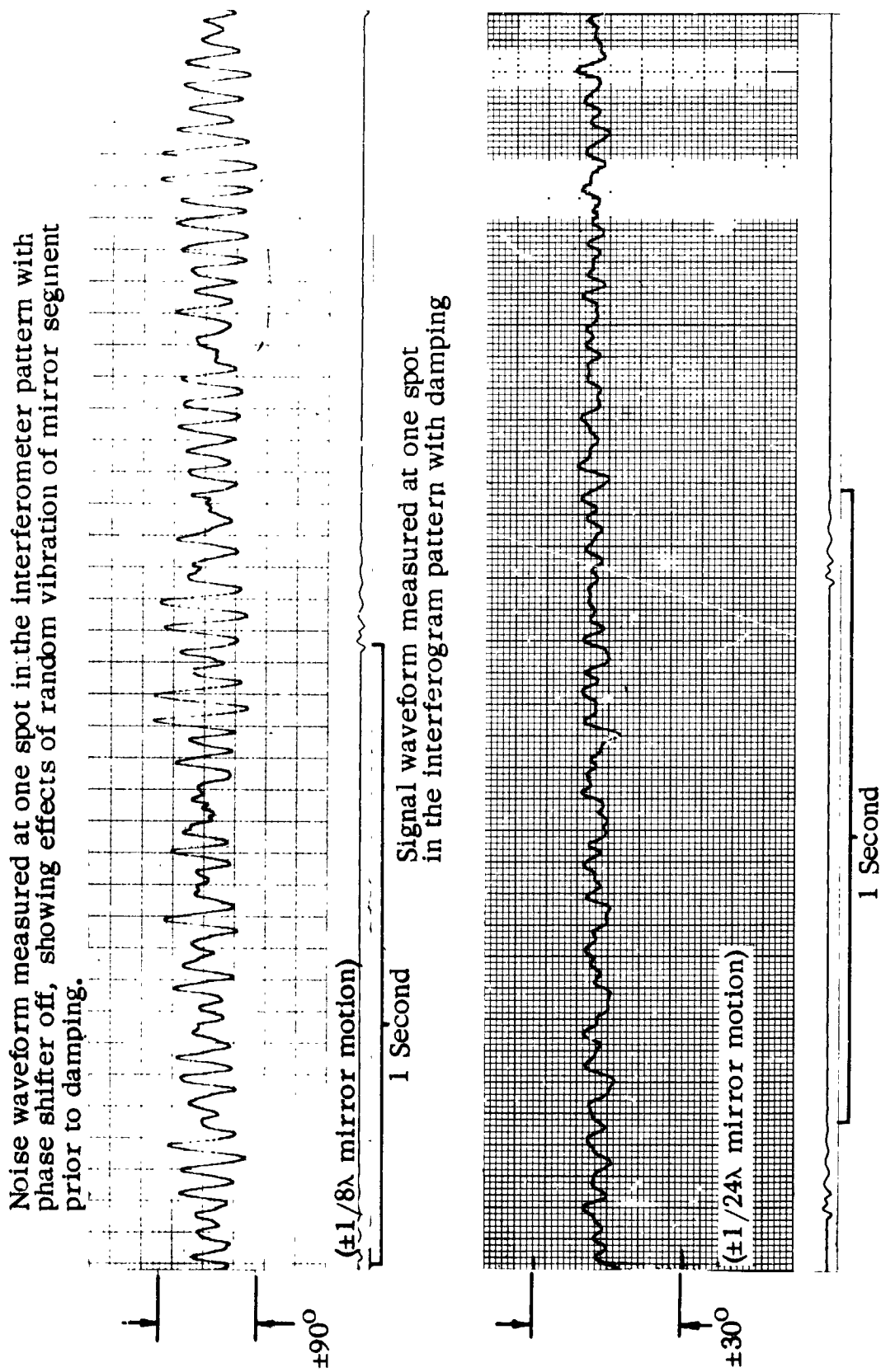
Figure 27. Random Vibration of Mirror Segment Before and After Damping
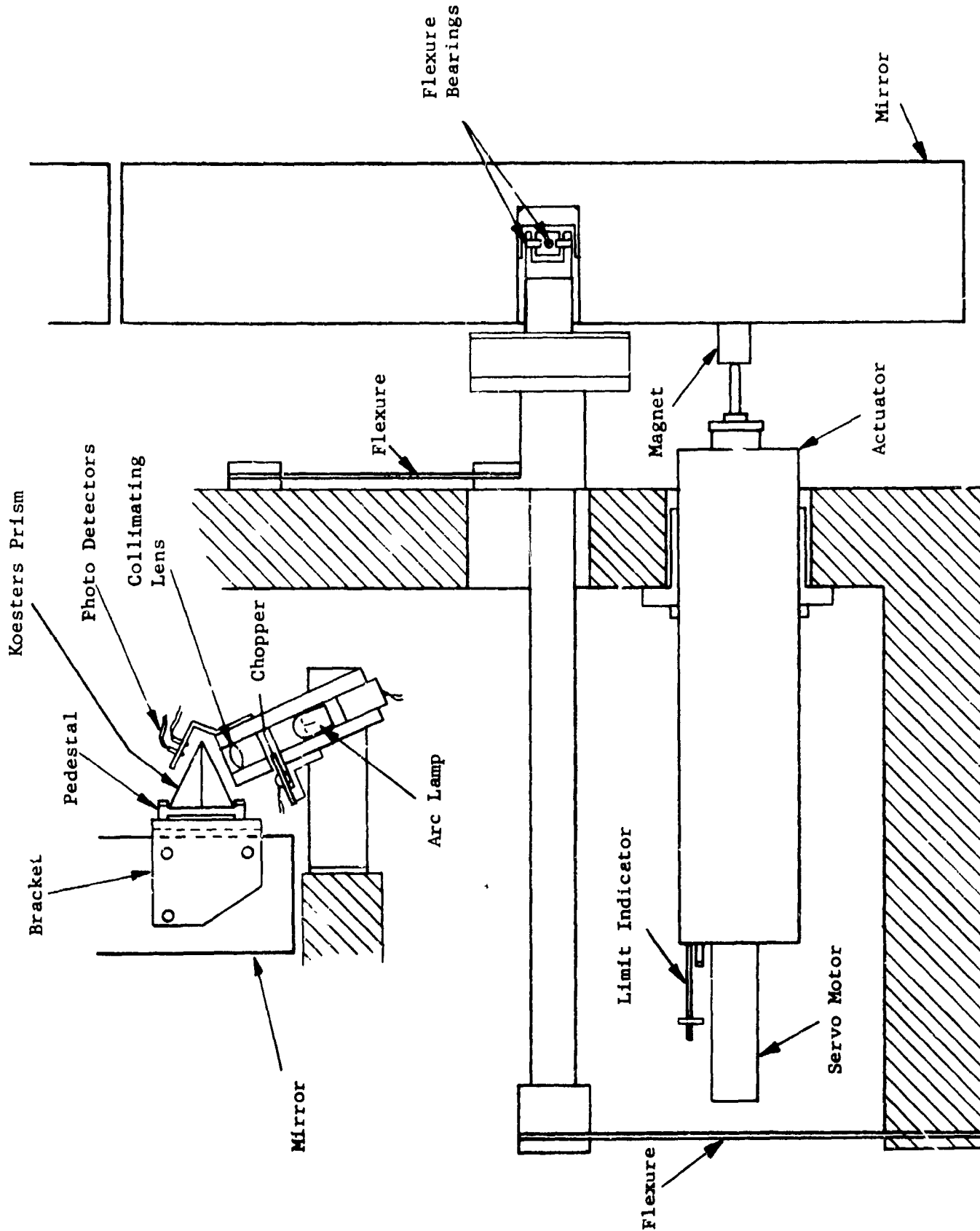
Figure 28. Mounting Arrangement Showing Mirror, Actuator, and White Light Interferometer Details

(Mirror is mounted with flexures so that motion in tilt and translation can be achieved with a minimum of friction)

This allows each mirror segment to be tilted a limited amount in two degrees of freedom, with a minimum of friction. The universal joint is on the end of a rigid rod which hangs by a leaf flexure from the main support frame. At the other end of the rod, another leaf flexure connects the rod and the main support frame and counters the weight of the mirror segment. These two leaf flexures allow a limited amount of mirror displacement parallel to the mirror axis, with a minimum of friction.

One face of each actuator flange is mounted flush against the main frame support and a threaded barrel allows each actuator to be positioned so that the mirror segments can be mechanically aligned to within a few thousandths of an inch. Magnets cemented to the backs of the mirror segments maintain the segments in contact with the actuators.

The white light interferometer Koesters prisms are mounted to the mirror segments with an L shaped bracket which mounts on studs cemented in holes drilled in the sides of the segments. The prisms are cemented to pedestals which are fastened to the L shaped brackets with screws, and the fine alignment of the prisms can be controlled by adjusting the tension on these screws. The remaining components of each white light interferometer, the light source, chopper, collimating lens and detectors are mounted together in a unit which is fastened to the main supporting frame rather than the mirror, in order to isolate their weight and vibration from the mirror segments.

The mirror, actuator, and white light interferometer assembly (see Figure 29) slides on two rails into one end of a vacuum tank. Mechanical stops on the rails allow the assembly to be easily removed and replaced to a fixed position. At the other end of the vacuum tank, the phase measurement interferometer and image scanner are assembled on a buttressed cantilever support which is rigidly mounted to the end of the vacuum tank. (See Figure 30.)

One point of concern at the outset of this experiment was the stability of the overall mounting assembly. It was clear that it would be necessary to do the experiment in a vacuum to avoid air turbulence. Therefore, a 36-inch diameter by 16-foot long vacuum tank was obtained. This tank was mounted on stabilized air-cushion vibration isolators. It was suspected, but not proven, that these mounts at times generated spurious transients which could be minimized by careful adjustment of the input air pressure to the servo system. During the Phase I testing, it was found expedient to place thermal isolation around the vacuum tank to minimize thermal drift and to eliminate acoustically coupled vibration. This was repeated for Phase II.

3.6 KNIFE-EDGE AND PINHOLE TEST ARRANGEMENT

Mirror figure measurements were performed on the composite mirror with knife-edge and pinhole tests conducted while the segments were being maintained in their proper positions by the closed loop servo system. The same 0.0002 inch pinhole source was used for both of these tests and was mounted 0.15 inch to one side of the center of curvature of the composite mirror. The error introduced by operating the pinhole this far off axis is equivalent to

Mirror segments, white light interferometers ( ), part of the
actuators, and supporting structure before being moved into
vacuum tank.

Figure 29. Mirror Assembly
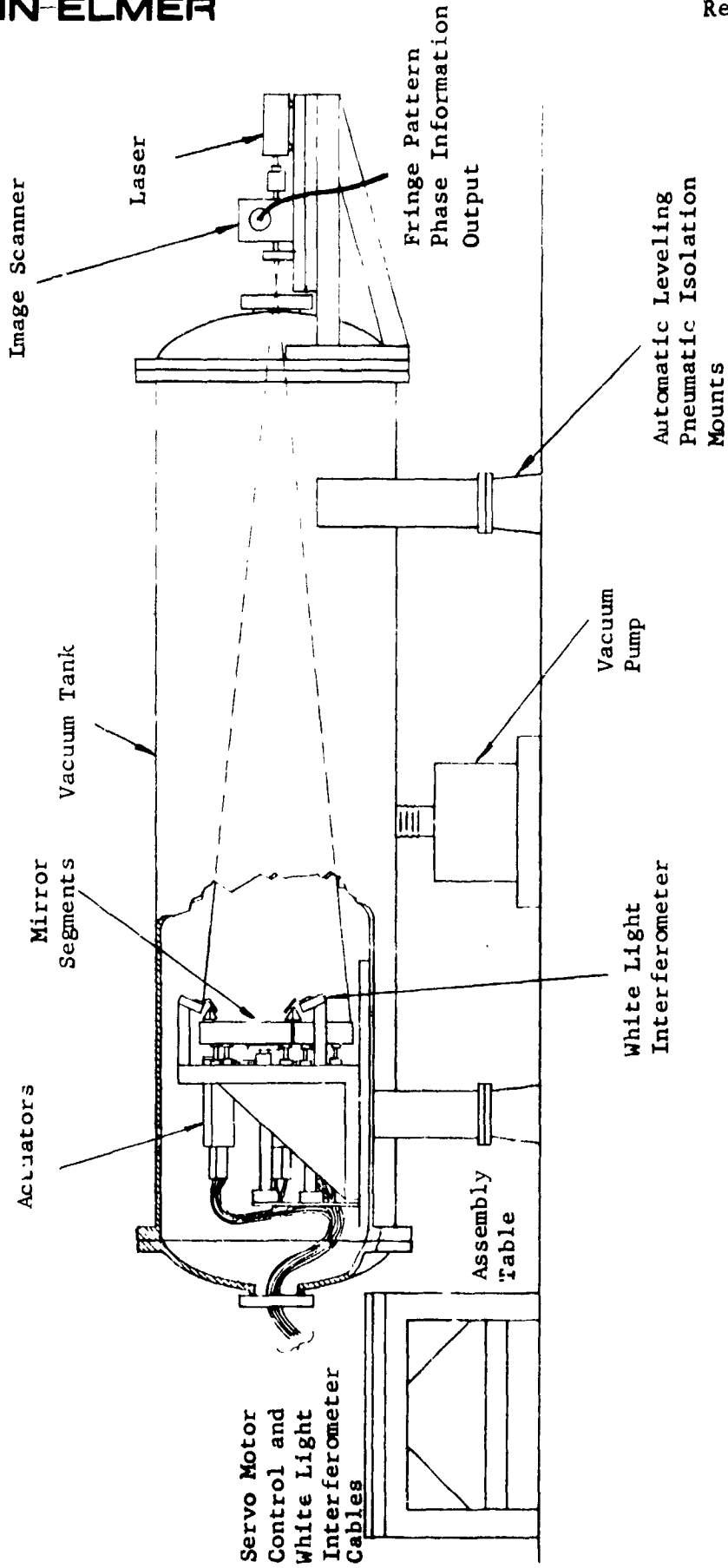
Figure 30. Experimental Assembly

an rms figure error of $\lambda/35$. The return beam is deflected upward by a small
45 degree mirror located on the other side of the center of curvature from
the pinhole and slightly towards the segmented mirror so that the beam is de-
flected before it comes to a focus and the focus is located slightly above the
axis of the system. A camera and microscope are positioned over this point to
observe either the image of the mirror for the knife-edge test or the image of
the pinhole for the pinhole test. The results of these tests are discussed in
Section 4.4 under Alignment Accuracy.

4.   SYSTEM PERFORMANCE

4.1   OPERATION

In operation, the control functions are at present sequenced manually by a set of control switches. This allows a flexibility of operation which is desirable in the present experiment where the system's reaction and response are being determined. The sequence of alignment operations is outlined in Table III. These steps can be best explained with reference to the functional diagram of Figure 31 and the scan pattern of Figure 19. The X-Y coordinates of the image dissector scanner are switched at a 3.3 kilocycle per second rate among 11 different locations in the image plane by an electronic multiplexing system. Ten of these locations are shown in the Scan Pattern of Figure 19. The eleventh location is a movable set of coordinates which can be located anywhere in the image plane or can be scanned between any two points in the image plane.

The sampled signals generated at each of the eleven individual sets of coordinates are reconstituted in the eleven-channel demultiplexer to eleven individual 60 cps sinusoidal waveforms which have the same relative phase as the corresponding points in the fringe pattern at the image plane.

The following is a step by step alignment procedure:

Step 1

Using the function selection switch and the coordinate selection switch, the movable point 11 is set to scan from point 1 to point 2. One of the phase detectors 11 inputs is connected to the output from demultiplexer 1. The other input to phase detector 11 is always connected to the demultiplexer 11 output. The output from phase detector 11 which is then proportional to the phase difference between point 1 and the moving point 11 is applied to servo amplifier 2. The actuator at point 2 will then produce a rotation of mirror segment I around the line between points 1 and 3 in a direction to reduce the phase difference between points 1 and 11. When point 11 arrives at point 2, point 2 will then have the same phase as point 1.

Step 2

The input of servo amplifier 2 is then connected to the output from phase detector 2 which is always proportional to the phase difference between points 1 and 2. Actuator 2 will then be continuously controlled to maintain the phase difference between points 1 and 2 as small as possible throughout all the following alignment operations.

TABLE III

Operating Sequence: Steps used for Alignment of Three Segments

| Step	Function	Operation	Interferometer	Reference Source	Actuators Driven
1	Segment I, Tilt Alignment	Sweep 1 to 2	φ Measuring	Spot 1	2
2	Segment I, Tilt Alignment	Lock 2 to 1	φ Measuring	Spot 1	2
3	Segment I, Tilt Alignment	Sweep 1 to 3	φ Measuring	Spot 1	3
4	Segment I, Tilt Alignment	Lock 3 to 1	φ Measuring	Spot 1	3
5	Segment I, Axial Alignment	Sweep 1 to 10	φ Measuring	Spot 1	1, 2, & 3
6	Segment II, Tilt Alignment	Sweep 4 to 5	φ Measuring	Spot 4	5
7	Segment II, Tilt Alignment	Lock 5 to 4	φ Measuring	Spot 4	5
8	Segment II, Tilt Alignment	Sweep 4 to 6	φ Measuring	Spot 4	6
9	Segment II, Tilt Alignment	Lock 6 to 4	φ Measuring	Spot 4	6
10	Segment II, Coarse Axial Alignment	Sweep 4 to 11	φ Measuring	Spot 4	4, 5, & 6
11	Segment II, Fine Axial Alignment	Axial Slew	White Light	-	4, 5, & 6
12	Segment II, Fine Axial Alignment	Lock Seg. II to Seg. I	φ Measuring	Spot 1	4, 5, & 6
3-19	Repeat 6 Through 12 for Segment III	——	——	4 and 1	7, 8, & 9
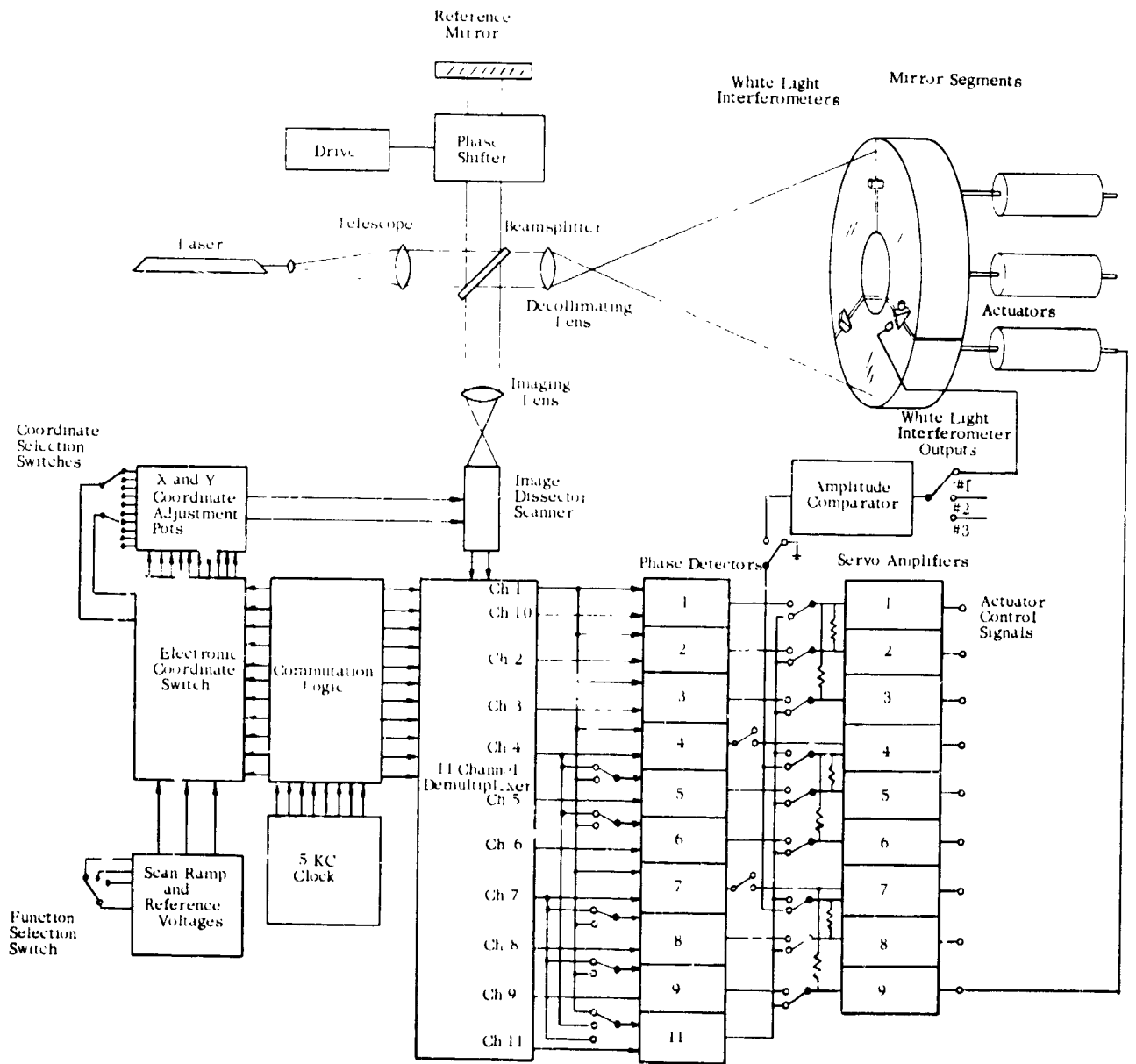
Figure 31. Function Diagram

Step 3

The coordinate selection switch and function selection switch are set to scan point 1₁ from points 1 to 3. The output of phase detector 11 is connected to servo amplifier 3. The input to phase detector 11 remains connected to demultiplexers 1 and 11. As point 11 scans from 1 to 3, actuator 3 will displace point 3 to reduce the phase difference observed between 1 and 11. When point 11 arrives at point 3, point 3 and point 1 will be in phase.

Step 4

The input of servo amplifier 3 is then connected to the output of phase detector 3. The phase difference between points 1 and 3 is also maintained as low as possible through the remaining operations.

Step 5

Segment I is now in tilt alignment, with points 1, 2, and 3 in phase. An axial misalignment of the segment can still exist, however. To reduce this error, point 11 is set to scan from points 1 to 10. The inputs of phase detector 11 are from points 1 and 11 and its output goes to servo amplifiers 1, 2, and 3 in parallel. Servo-amplifiers 2 and 3 also remain connected to phase detectors 2 and 3 respectively so that points 2 and 3 are being maintained in phase with point 1. Therefore, any output from phase detector 11 representing a phase difference between points 1 and 11 will cause the entire segment I to translate in a direction parallel with a line drawn from point 10 to the center of curvature of the composite mirror until the phase difference is reduced. When point 11 arrives at point 10 at the end of the scan, point 10 will be in phase with points 1, 2, and 3 and segment I will be in alignment.

Steps 6-10

For the alignment of segment II steps 6 through 10 are a repetition of 1 through 5 with substitution of spots 4, 5, and 6 for spots 1, 2, and 3. The sensitivity of axial alignment is such that several wavelengths of relative axial phase difference can still exist between segments when the phase difference between points 4 and A has been minimized.

Step 11

To reduce the remaining relative axial displacement between segments I and II, the white light interferometer is turned on and segment II is translated axially by driving actuators 4, 5, and 6 until the interferometer indicates alignment between the segments. Since the white light interferometer does not have directional sense, it may be necessary to limit cycle the motion of segment II to find the alignment. The alignment of the two segments will be within 1/4 wavelength at the conclusion of this step.

Step 12

To reduce the relative alignment of segments I and II to a small fraction of a fringe, the input to servo amplifier 4 is connected to the output

from phase detector 4.   The relative phase of points 1 and 4 then controls
actuator 4.   The inputs to phase detectors 5 and 6 are then switched from point
4 to point 1 and points 2, 3, 4, 5, and 6 will all be locked in phase to point 1.
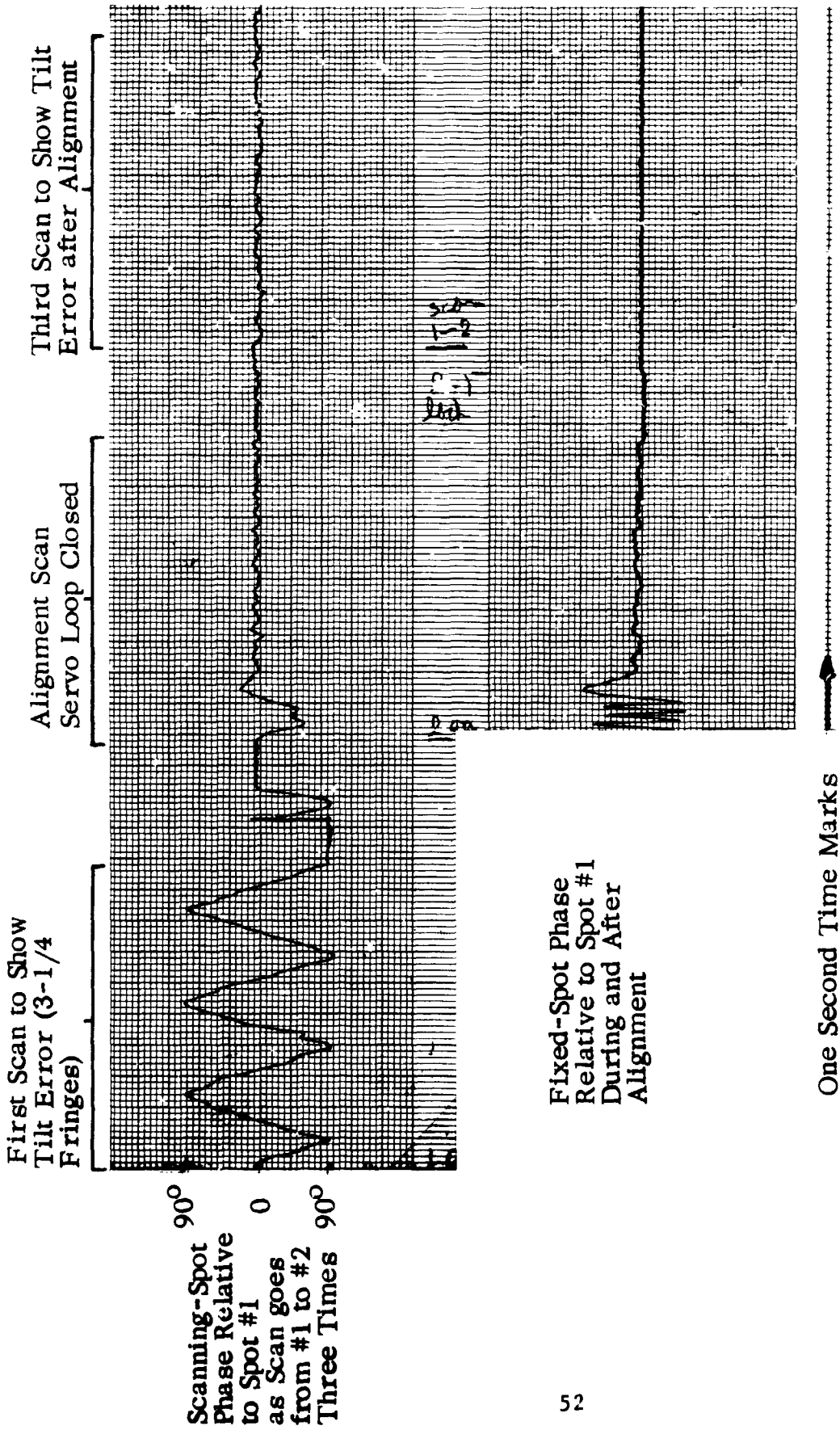
Steps 13-19

Steps 6 through 12 are repeated for segment III until finally all points
2, 3, 4, 5, 6, 7, 8, and 9 are locked in phase with point 1.

4.2 TILT ALIGNMENT

As described in the foregoing, tilt alignment is performed in two
steps per segment.   The following will describe a typical tilt alignment opera-
tion.   In this experiment, segment I was initially misaligned in tilt about the
1-3 axis by 3-1/4 fringes.   This was done by manually driving actuator 2.   The
alignment experiment then consisted of: (1) scanning the fringes to indicate
tilt error; (2) automatic servo controlled tilt alignment; and (3) repeating
the same scan as in (1) to show that all fringes have been wiped out, while
leaving servo 2 on.   Figure 32 is a record of this experiment.   The top trace
shows the output of phase detector 11 for all three steps.   This is the detector
which compares the phase of the scanned spot to the phase of spot 1.   The bottom
trace shows the output of phase detector 2 which compares the fixed spot 2 with
spot 1.   The first scan of phase detector 11 shows the 3-1/4 fringes of tilt
error.   In the second scan, phase detector 11 generates an error signal which is
used to control actuator 2.   Also, during the second scan, the bottom trace of
Figure 32 indicates the displacement of spot 2 caused by actuator 2.   It can be
seen that the three fringes are wiped out early in the scan.   The third scan of
phase detector 11 then shows residual figure error due to the mirror imperfec-
tions only, while the bottom trace shows the stability of the tilt loop servo
operation.

Figure 33 shows a similar sequence of alignment.   In this case, the
initial misalignment amounted to 23 fringes and a slower sweep rate was used.
In an actual application of the active optics technique, it would be desirable
to use an exponential sweep rate for tilt alignment.   This would permit correc-
tion of tilt errors amounting to 100 fringes or more.

After wiping out fringes in tilt, the servos are left on with spot 2
locked in phase to spot 1.   The accuracy and frequency response of this tilt
servo loop was examined.   Figure 34 shows the gain constants for the tilt servo
loops.   From these, it can be calculated that the open loop gain will be unity
at approximately 1 cps.   Figure 35 shows the calculated open loop gain and phase
characteristic.   Figure 36 shows the measured closed loop frequency response.
The rise in this response at approximately 1/2 cps was more than anticipated.
This difference is attributed to an unexpected spring constant in the 227 to 1
gear train.   Figure 37 shows the corresponding time response obtained by insert-
ing a square wave forcing function into the servo motor control loop.   This
indicates that small external disturbances with periods of 1 second or larger
can be accommodated.   More rapid impulse transients will normally not affect
the operation.   However, more rapid unit step transients will result in misalign-
ment of an integral number of 1/2 wavelength which must be corrected by repeating

Figure 32. Tilt Alignment Performance

Figure 33.   Tilt Alignment Performance

Repeat of Figure 32 with 23 fringes of tilt error, and a slower alignment scan.

Figure 34. Tilt Alignment Servo Diagram
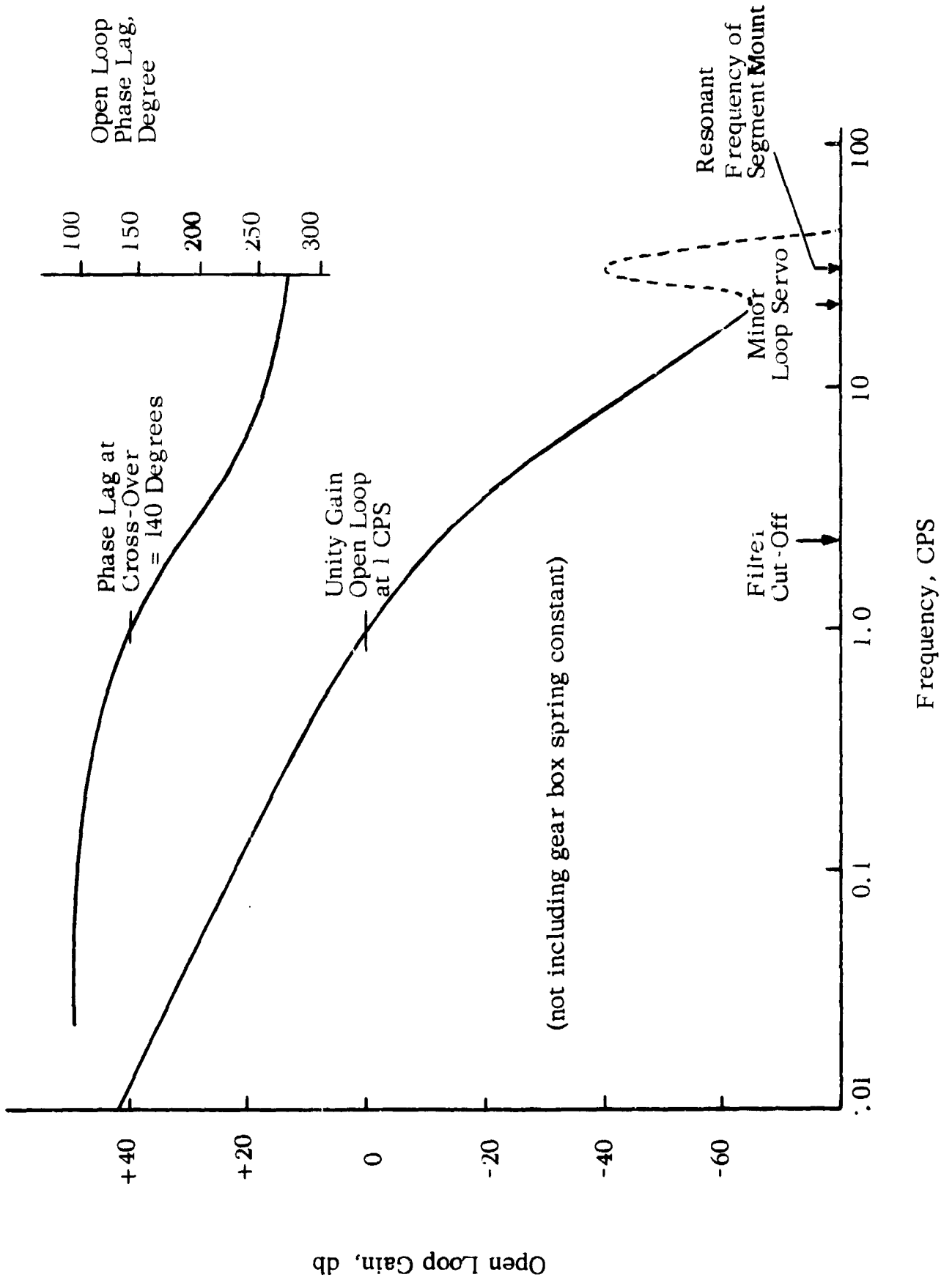
Figure 35. Tilt Servo Open Loop Frequency Characteristics
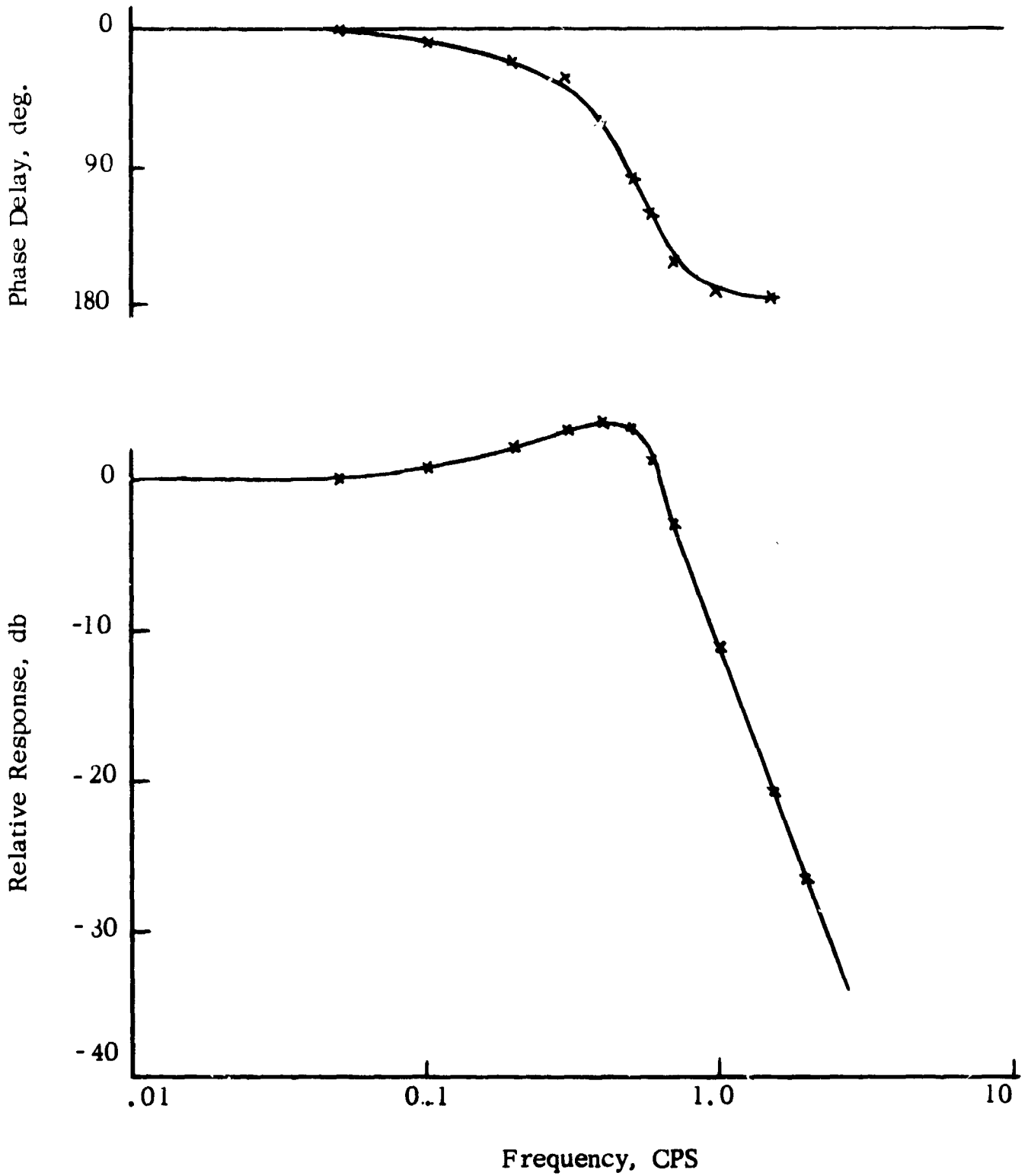
Figure 36. Tilt Servo Closed Loop Frequency Response

**Servo Amplifier
Control Signal**

**One Second
Time Marks**
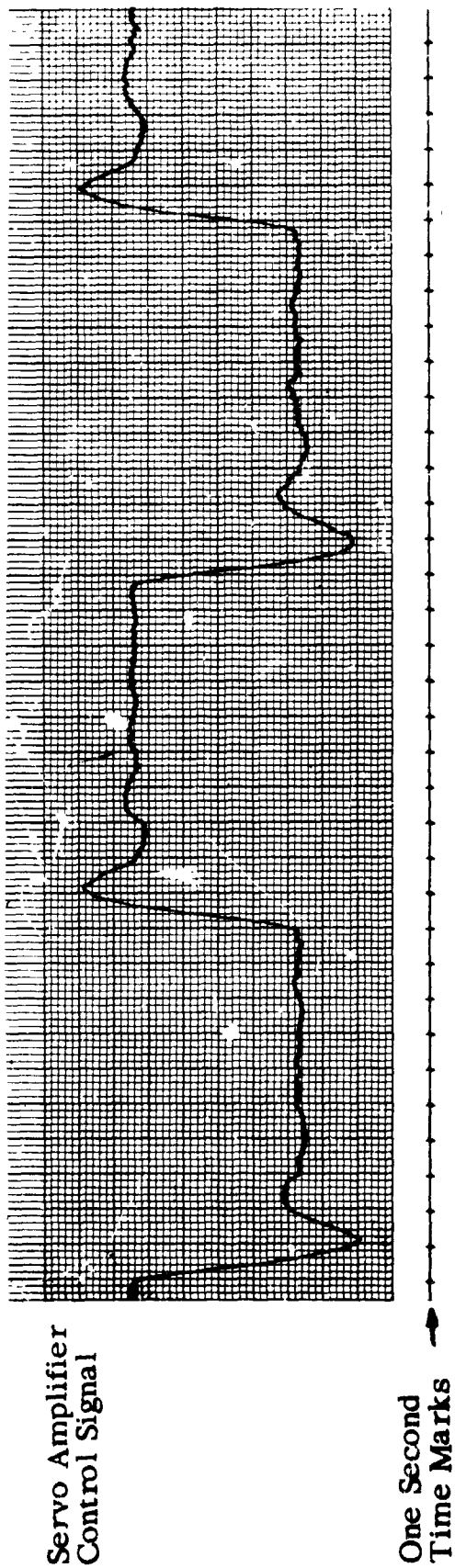
Obtained by introducing a square wave disturbance into servo amplifier
and recording the compensating voltage generated by the tilt alignment
servo.

Figure 37. Tilt Servo Closed Loop Time Response

57

the alignment procedure, or by the use of a fringe counting logic capable of memorizing a transient error and reading out an appropriate control signal.

In the course of testing, it was found that some actuators had a small spring constant in the gear box. This in effect introduced a small dead zone in the servo control, approximately 1/2 microinch equivalent at the output. As a result, the tilt loop servo using these actuators at times limit cycled about this dead zone. Figure 38 shows examples of proper and improper operation.
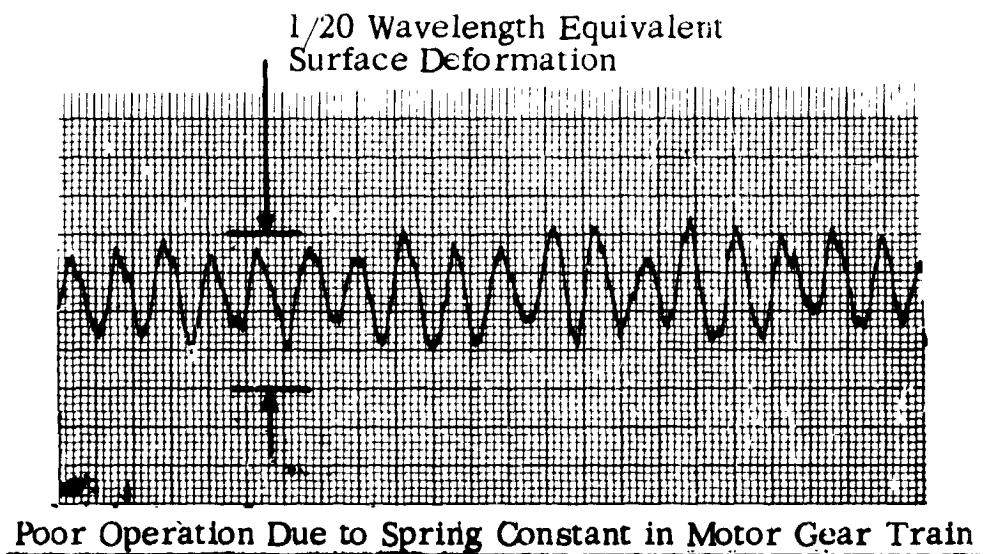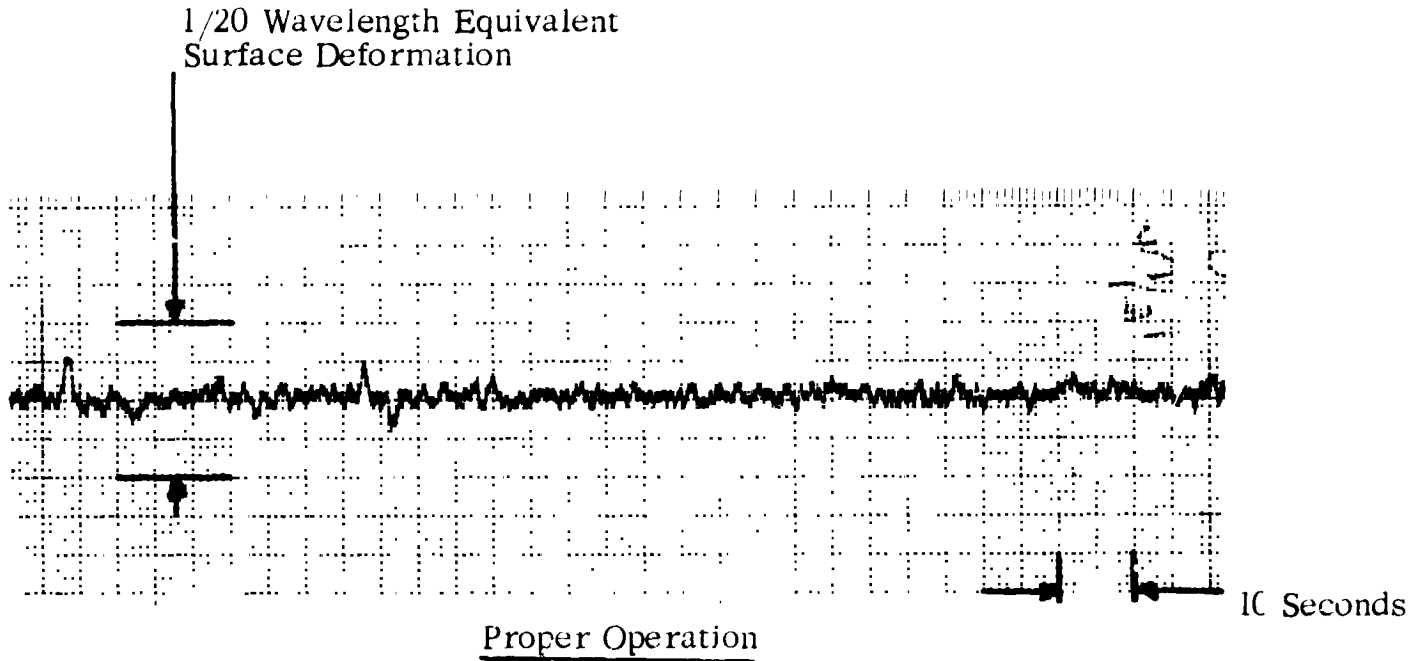
4.3 AXIAL ALIGNMENT

Alignment of the segment in the axial dimension requires two separate functions. After segment I has been aligned in tilt, points 1, 2, and 3 will be at the same phase on the phase measuring interferometer fringe pattern. In the absence of error, the complete fringe pattern will be equiphased over the whole segment. In the presence of an axial error, the fringe pattern will contain circular fringes centered at point 10. The magnitude of the axial error signature for the geometry used in this experiment is: when the segment center of curvature is displaced axially from point "C" by 400 wavelengths (0.01 inch) one fringe will appear between spots 1 and 10. Most of the experimental work was done with less than one fringe of axial misalignment. It normally required approximately ten minutes to go through this portion of the alignment procedure. Records of this operation were taken but are too lengthy to incorporate into this report. Initially, it was hoped that this adjustment could be accomplished automatically to an accuracy of 1/100 fringe which would result in axial alignment accuracy of ±4 waves. A practical number appears to be closer to ±30 waves relative to point "C" in Figure 7.

The second step of axial alignment procedure consists of locating segments II and III co-planar to segment I, using the white light interferometer. Figure 13 showed the signature of the white light interferometer. Figure 39 shows utilization of this signature to control the position of segment II relative to segment I. The top trace of this figure indicates relative segment position, where each large cycle corresponds to one fringe, or a 12 microinch change in position of segment II. The bottom trace is of the white light interferometer output. The lefthand portion of each trace is taken during segment 2 drive. When the two segments are almost equidistant from the white light interferometer, the electronic output goes from minus to plus. This voltage change is used to stop the drive and to lock the reference spot of segment II to the reference spot of segment I, i.e., lock spot 4 to spot 1. This servo action then reduces the relative displacement between the two segments to a small fraction of a wave.

4.4 ALIGNMENT ACCURACY

Several types of data were collected to indicate the overall alignment accuracy and stability.

- Pinhole image photographs
- Knife-edge test photographs
- Phase measuring interferometer recording
- Interferometer fringe pattern photographs

1/20 Wavelength Equivalent
Surface Deformation

Proper Operation

1/20 Wavelength Equivalent
Surface Deformation

Poor Operation Due to Spring Constant in Motor Gear Train

Showing the random fluctuations of one spot on the mirror relative to a reference spot as a function of time for closed loop tilt control; examples of proper and poor operation.

Figure 38. Tilt Loop Stability
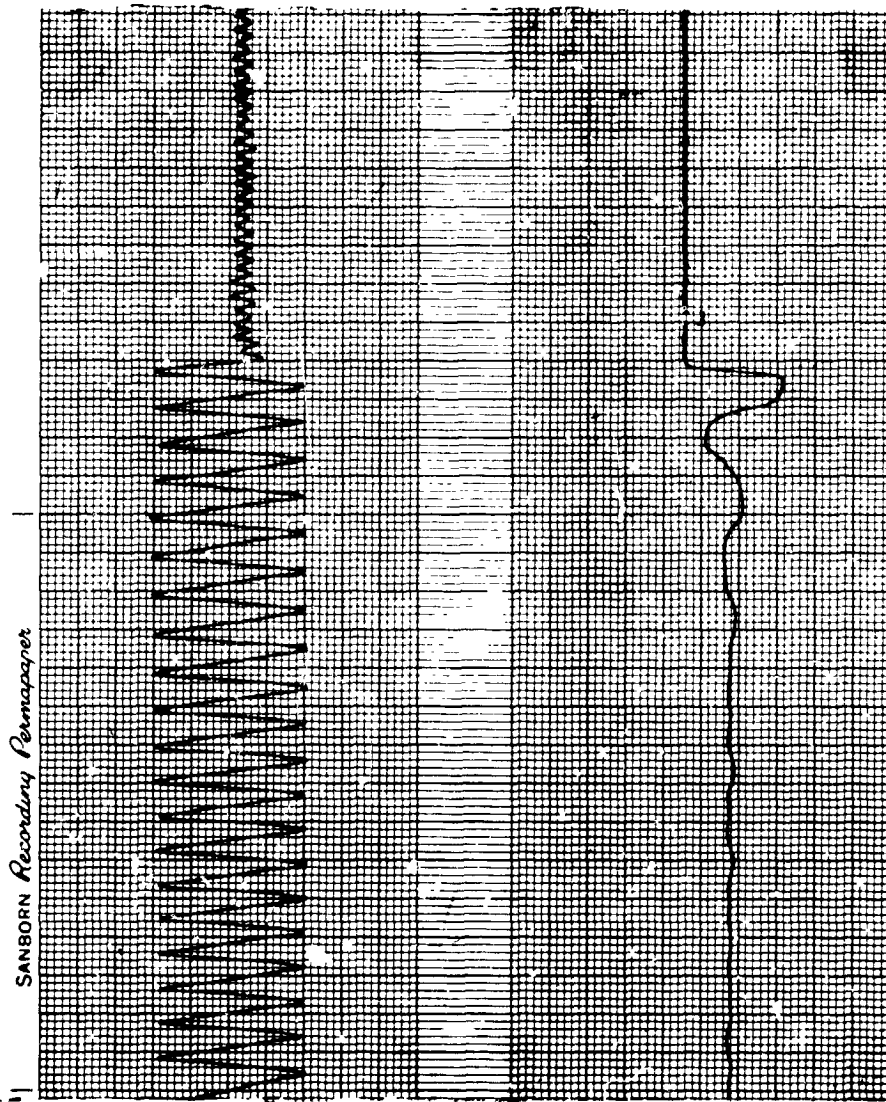
Figure 39. Ambiguity Sensor Operation

Showing first the fringes generated by slewing segment II relative to I and second the control signal for positioning segment II relative to I. (Including a small servo limit cycling.)

Examples of this data are given in Figures 40 through 43. Except for the fringe patterns, the data was taken while the system was in operation. The knife-edge and pinhole tests, although only qualitative in nature, do indicate good performance. The phase measuring interferometer recordings of Figure 42 are somewhat compromised by the figure errors in the interferometer parts. Where these errors peak at a control spot they affect performance but do not show in the scan recordings. This could introduce up to 1/40 wavelength additional error. The average figure error indicated by Figure 42 is 1/40λ. The rms value for random small scale errors would be approximately 1.25 times this value.

The fringe patterns of Figure 43 were obtained before and after alignment. To obtain these photographs, it was necessary to turn off the phase shifter and control servos during the test. This permitted a small amount of drift before the picture was taken. The bottom patterns were obtained by tilting the reference mirror in the interferometer. Perfect alignment with a perfect mirror would result in straight fringes across the full diameter of the mirror, bridging all segment intersections.

Estimates have been made from the data collected of overall performance. The results are shown in Table IV. The focus and tilt numbers are obtained from the nine control spots only. The composite average figure error of this experiment is estimated to be between 1/30 and 1/40 wavelength. This number is obtained from an integration over the entire mirror and includes the effects of the turned down edges at the circumference and at the segment cuts plus an estimate for the contribution due to the figure sensor. These numbers compare quite favorably with the design objective of 1/20 wavelength rms.

1/16 Sec. Exp.   1/4 Sec. Exp.

4 Sec. Exp.   15 Sec. Exp.
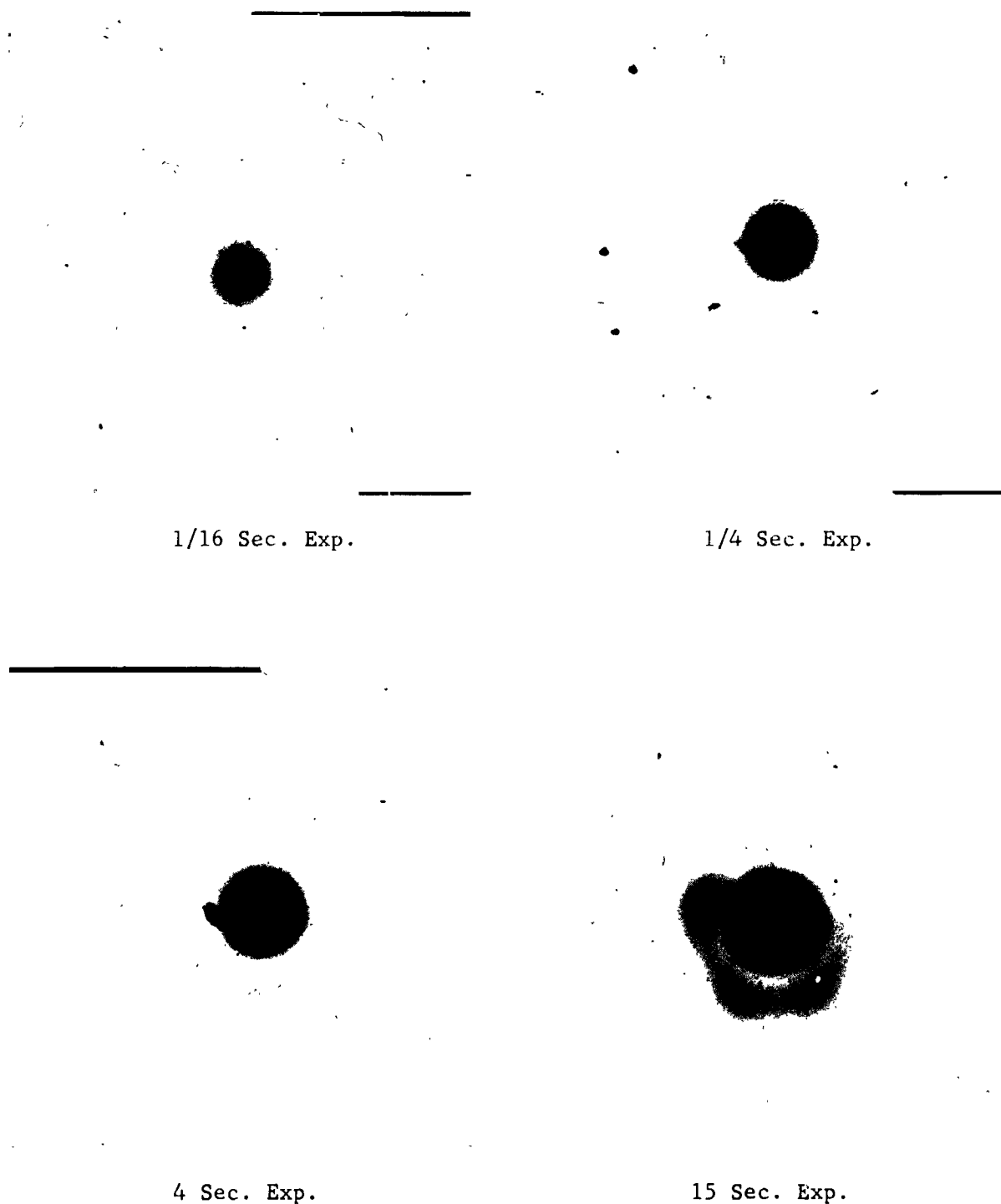
0.002" Pinhole diameter, tungsten source Kodak Plus X
developed 4 min. in D76. Total enlargement 2500X.

Figure 40. Pinhole Images

Figure 41. Foucault Knife-edge Test. Made After
Alignment and with Control System Operating
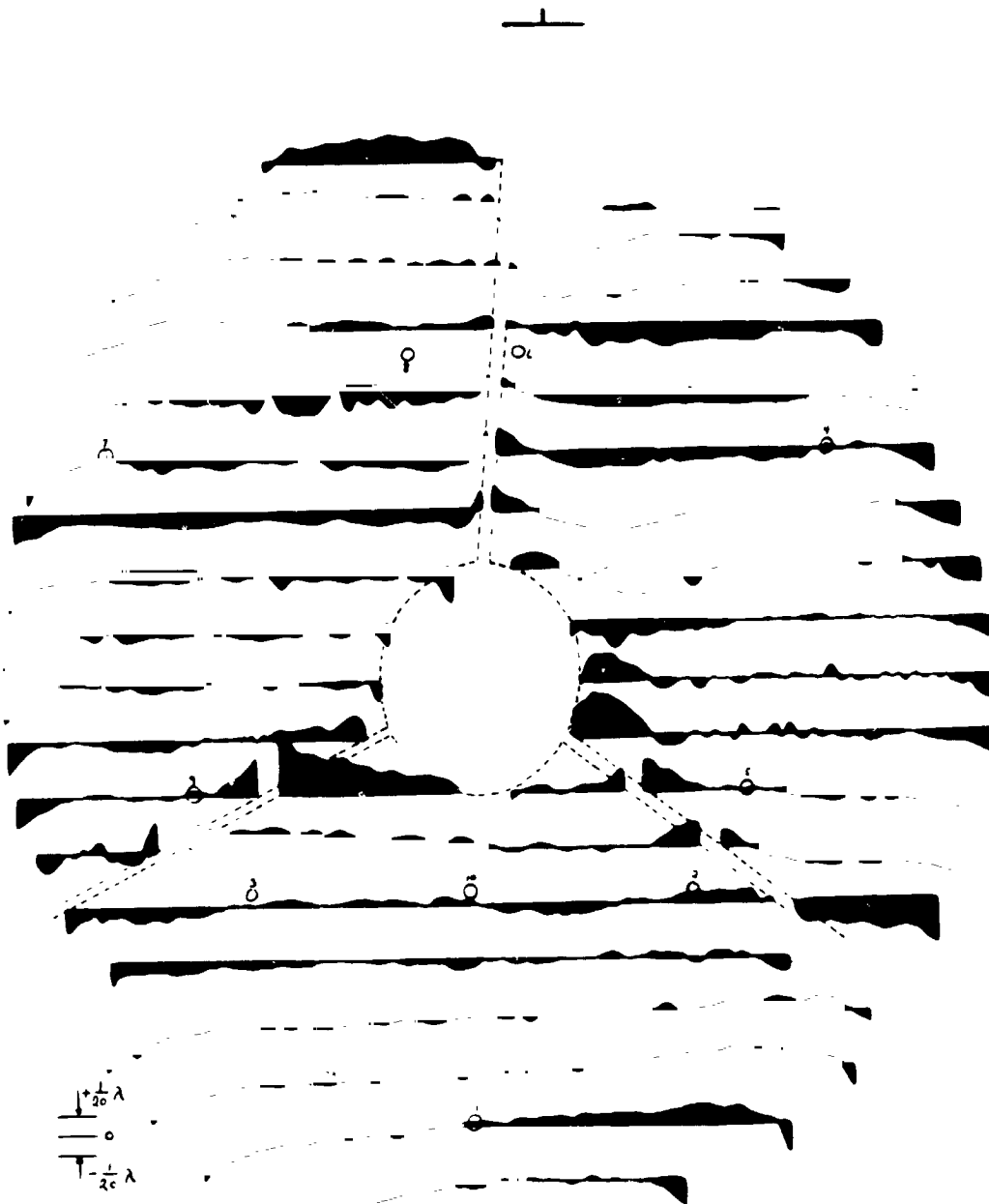
Figure 42.   Figure Error Profiles

This was prepared from an average of three raster scans of
composite mirror while control system was in operation.   Data
was obtained from scanning spot of phase measuring interfero-
meter.   Figure error determined by integration of profiles is
1/40 wavelength average.

Before Alignment

After Alignment with Various Phase of
Interference Taken From Phase Measuring
Interferometer with Phase Shifter Off

After Alignment with Tilt
Introduced in Reference
Beam of Interferometer

Figure 43.   Mirror Fringe Patterns Before and After Alignment

TABLE IV

ALIGNMENT ACCURACY

| | TILT | | AXIAL | | COMPOSITE |
	ACCURACY	STABILITY	ACCURACY	STABILITY	FIGURE ERROR
Experimental Measurements	1/20λ p-p	1/70 to 1/200 λrms	±30λ absolute, 1/20λ p-p relative between segments	1/35λ/min.	1/30 to 1/40λ Average
Experimental Limiting Factors	Spurious reflections and figure of interferometer parts.	Small limit cycle in some servo loops.	Figure of interferometer and mirror plus servo loop limit cycle	Vacuum tank dimensional stability	Interferometer parts.
Fundamental Limiting Factors	Photon Noise in Figure Sensor	Photon Noise in Figure sensor	Photon Noise in Figure Sensor	Dimensional Stability of structure between mirror and figure sensor	Photon Noise

Note: One wavelength, λ, is 24 micro-inches

66

5.   RECOMMENDATIONS

        The concept of Active Optics has been proven in the laboratory,
however, there is much to be done before it can be said that this technique
is ready to fly in a spaceborne system. It is recommended that this work be
continued along several lines. Further component development is required to
perfect the figure sensor and to derive an actuator concept suitable for long-
life operation in a space environment. A comparable laboratory evaluation
of the Active Optics concept as applied to a single, relatively thin, and
deformable mirror should be undertaken. A logical next step would be to find
and solve those problems associated with applying these same techniques to a
large aperture mirror of a size which might conceivably be considered for
future spaceborne astronomical telescopes. It is none too soon to begin
thinking about this work if this technology is to support the recommendations
of the National Academy of Sciences and the National Aeronautics and Space
Administration in the "Woods Hole" report, "Space Research - Directions for
the Future."

        In order to apply the segmented Active Optics principle to a space-
borne telescope, refinement of the present components and investigations along
the following lines are indicated.

MIRROR CONSIDERATIONS

        The present contract has been primarily concerned with demonstrat-
ing the technique for positioning mirror segments using a closed loop servo
system, and to avoid complicating this experiment, a single 20-inch spherical
mirror cut into three parts was used as the segmented primary. In an actual
telescope, an aspherical primary mirror probably would be desired, however,
the mirror would be so large that it would be impractical to make it in one
piece and then cut it into segments. The mirror, therefore, probably would
be figured in segments and some of these would be off-axis sections of an
aspheric surface. The development of new techniques for fabrication of these
off-axis diffraction-limited aspherics is indicated. However, we feel that
this particular problem will not be a critical one.

        Another problem introduced by the use of an aspherical primary
results from the fact that a single point center of curvature does not exist.
The use of a null corrector lens to eliminate this problem will allow the
phase measurement interferometer to be used just as effectively for an as-
pheric as for a spherical mirror.*

        Aspherical segments require one more degree of position control
than spherical segments, in a radial direction perpendicular to the mirror
axis. This lateral positioning does not appear to be a problem, however, even

---

*A. Offner, "A Null Corrector for Paraboloidal Mirrors," Applied Optics, Feb., 1963.

for very short focal lengths. The lateral control of position required to prevent an rms degradation of figure of greater than $\lambda/50$ for a 120-inch diameter parabolic mirror made up of 40-inch segments has been calculated for several different focal lengths:

F no.	Lateral Control Necessary
f1	less than 2.4×10^{-3} inches
f2	less than 21×10^{-3} inches
f3	less than 72×10^{-3} inches

COMPONENT CONSIDERATIONS

Most of the components need engineering improvement and space qualification; this includes the laser, the phase measurement interferometer, the white light interferometer, and the image scanner. The need for further development of actuators as a key component of an Active Optical system has been indicated. A coarse positioning scheme which can be completely auto- mated has been described in Section 3.2.3 but has not been tested.

A figure sensor which operates at the optical focus instead of at the center of curvature might be desirable to reduce the overall telescope length requirement. A new concept is needed if this is to be done. The ef- fect of a figure sensor located at the center of curvature on the telescope length may be somewhat mitigated, however, by the possibility that an active primary mirror might be constructed and operated at a shorter focal length than one using a conventional monolithic mirror of the same diameter. Fur- thermore a figure sensor located away from the optical focal plane is less likely to interfere with other instruments at the focal plane.

A final recommendation concerns further evaluation of the Active Optics concept. The present project used a segmented mirror approach. A com- parable laboratory investigation should be undertaken to determine the relative merits of a single, relatively thin, deformable mirror approach. The objective of this work should be to provide sufficient data to make possible an engineering selection of the most suitable Active Optics scheme for the design of the pri- mary mirror in a large orbiting telescope.